Thermal Structure of Eastern Australia's Upper Mantle and Its Relationship to Cenozoic Volcanic Activity and Dynamic Topography

P. W. Ball[1,2] , K. Czarnota[3] , N. J. White[1] , M. Klöcking[2] , and D. R. Davies[2]

[1]Department of Earth Sciences, University of Cambridge, Cambridge, UK, [2]Research School of Earth Sciences, Australian National University, Canberra, Australia, [3]Geoscience Australia, Canberra, ACT, Australia

Abstract Spatio-temporal changes of upper mantle structure play a significant role in generating and maintaining surface topography. Although geophysical models of upper mantle structure have become increasingly refined, there is a paucity of geologic constraints with respect to its present-day state and temporal evolution. Cenozoic intraplate volcanic rocks that crop out across eastern Australia provide a significant opportunity to quantify mantle conditions at the time of emplacement and to independently validate geophysical estimates. This volcanic activity is divided into two categories: age-progressive provinces that are generated by the sub-plate passage of mantle plumes and age-independent provinces that could be generated by convective upwelling at lithospheric steps. In this study, we acquired and analyzed 78 samples from both types of provinces across Queensland. These samples were incorporated into a comprehensive database of Australian Cenozoic volcanism assembled from legacy analyses. We use geochemical modeling techniques to estimate mantle temperature and lithospheric thickness beneath each province. Our results suggest that melting occurred at depths ≤80 km across eastern Australia. Prior to, or coincident with, onset of volcanism, lithospheric thinning as well as dynamic support from shallow convective processes could have triggered uplift of the Eastern Highlands. Mantle temperatures are inferred to be ~50–100°C hotter beneath age-progressive provinces that demarcate passage of the Cosgrove mantle plume than beneath age-independent provinces. Even though this plume initiated as one of the hottest recorded during Cenozoic times, it appears to have thermally waned with time. These results are consistent with xenolith thermobarometric and geophysical studies.

Plain Language Summary Earth's convecting mantle lies between the tectonic plates and the core. This mantle layer circulates, driven by the rising and sinking of hot and cold material, respectively. These internal motions can push the tectonic plate above up or down, generating surface topography. Here, we propose that the Eastern Highlands of Australia formed in response to hot mantle displacing cold mantle at the base of the Australian plate. We arrive at this conclusion using observations gleaned from Australia's volcanic past. Vast amounts of volcanic activity has occurred across Eastern Australia over the last sixty million years. We use the chemical composition of volcanic rocks to estimate mantle temperatures present at the time of eruption. We find that volcanic activity was initiated by wholesale emplacement of hot mantle beneath Eastern Australia, and that this event was coincident with uplift of the Eastern Highlands. However, the largest volcanoes in Eastern Australia developed above localized conduits of especially hot mantle material, known as plumes. Plumes rise from great depths and remain stationary. Therefore, since Australia has moved northwards during Cenozoic times, these larger volcanoes have formed in chains beginning near Townsville 40 million years ago, and ending near Melbourne five million years ago.

1. Introduction

Spatial and temporal changes to the thermal structure of the upper mantle beneath Australia exert a primary control on the distribution of mineral deposits, geothermal heatflow, dynamic topography, relative sea-level fluctuations, and clastic sedimentary flux onto adjacent continental margins (e.g., Czarnota et al., 2013, 2014; Hoggard et al., 2020; Müller et al., 2016; Salles et al., 2017; Sandiford, 2007). In this region, existing models of this thermal structure rely upon either xenolith thermobarometry, seismic tomographic imaging, or some combination of both (e.g., Davies & Rawlinson, 2014; Fishwick & Rawlinson, 2012; Hoggard et al., 2020; Kennett et al., 2013; O'Reilly & Griffin, 1985). These models are incomplete since xenolith thermobaromet-
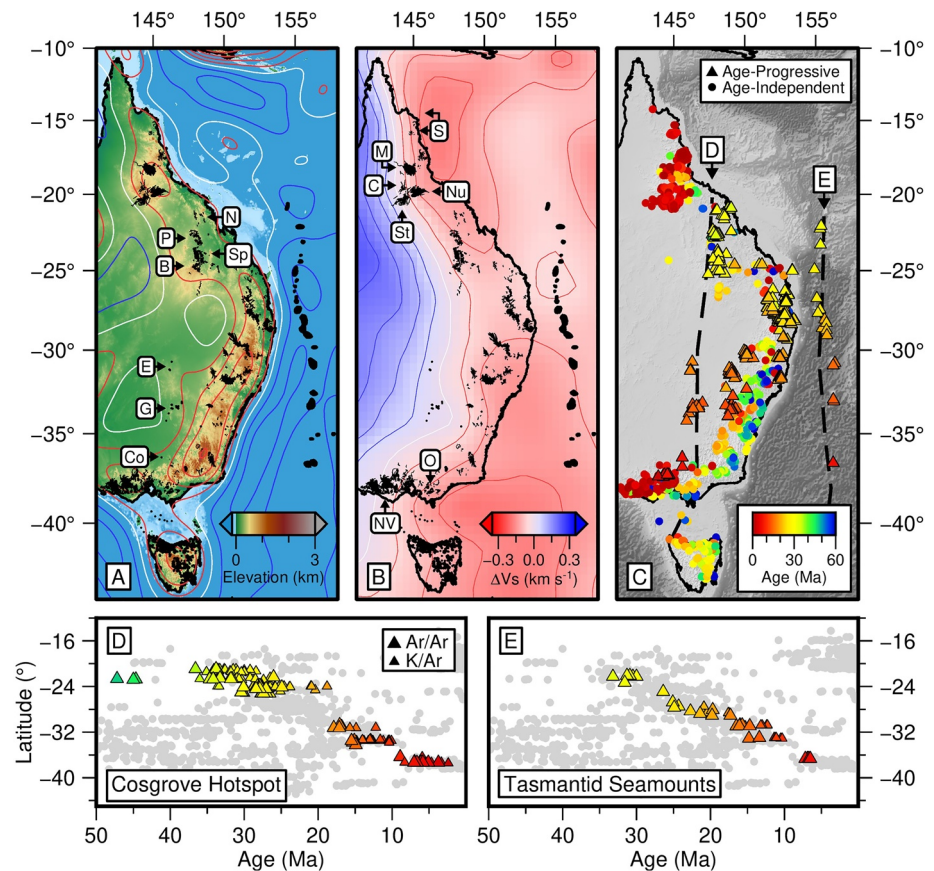
Figure 1. Tectonic setting of eastern seaboard of Australia. (a) Topographic map with lettered boxes showing main age-progressive volcanic provinces (see Table 1 for provincial names). Red/white/blue contours = positive/zero/negative free-air gravity anomalies at 10 mGal intervals from DIR-R5 database, low-pass filtered for wavelengths >800 km (Bruinsma et al., 2014). Black polygons = loci of Cenozoic volcanism (Raymond et al., 2012). (b) Shear-wave velocity averaged between 100 and 200 km depth from global tomographic model together with principal age-independent volcanic provinces (see Table 1 for province names; Schaeffer & Lebedev, 2013). Shear wave velocity shown relative to a reference model (Schaeffer & Lebedev, 2013). Red/white/blue contours = negative/zero/positive ΔV_s at 0.05 km s^{-1} intervals. (c) Location of dated intraplate volcanic samples, colored by age. Triangles = age-progressive volcanic samples; circles = age-independent samples (Data Set S1); dashed lines = flow lines constructed by tracking motion of Australian plate relative to Pacific hotspot reference frame (Matthews et al., 2016). (d) Radiometric dates as function of latitude for Cosgrove hotspot track. Large/small colored symbols = ^{40}Ar–^{39}Ar/^{40}K–^{40}Ar and ^{14}C dates; gray symbols = Cenozoic radiometric dates for eastern Australia. (e) Same as panel D for Tasmantid hotspot track.

ric constraints offer limited spatial coverage and tomographic models have coarse spatial resolution and cannot image past mantle structure. In order to improve our understanding of the way in which Australian upper mantle structure influences surface processes, a greater range of disparate observations is required to constrain lithospheric thickness and asthenospheric temperature as a function of geologic time.

Analysis of the chemical composition of basaltic lavas provides an important means for investigating upper mantle structure (Klein & Langmuir, 1987; McKenzie & O'Nions, 1991). Since Late Cretaceous times, the eastern seaboard of Australia has experienced extensive intraplate volcanism. This volcanism coincides with the Eastern Highlands, which are a series of elevated plateaux and mountain ranges that run parallel to the seaboard (Figure 1a). Coincidence of this physiography with positive long-wavelength free-air gravity anomalies and with slow shear-wave velocity anomalies within the upper mantle, suggests that sub-crustal processes contribute both to volcanism and to topography (Figures 1a and 1b; Czarnota et al., 2014; Wellman, 1979, 1987).

There is no unified quantitative understanding of this Cenozoic magmatic activity, which can be sub-divided into four categories: offshore seamount chains, central volcanoes, leucitites, and lava fields (John-
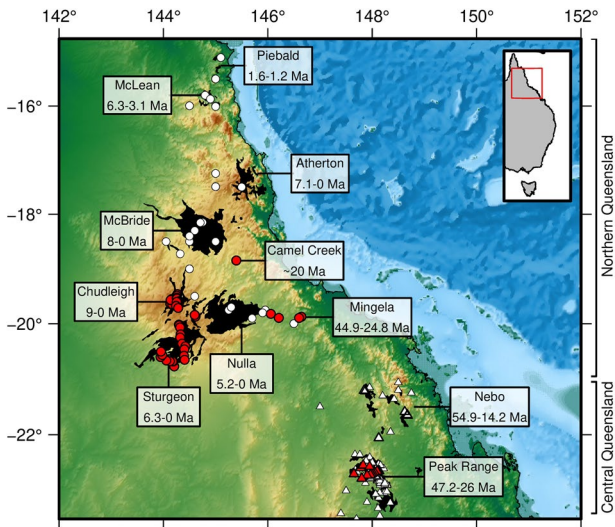
Figure 2. Topographic map of northern and central Queensland showing chronology of Cenozoic volcanic provinces (Cohen et al., 2017; Coventry et al., 1985; Gibson, 2007; Griffin & McDougall, 1975; Johnson, 1989; Jones et al., 2020; Stephenson & Griffith, 1976; Stephenson et al., 1998; Whitehead et al., 2007; Wyatt & Webb, 1970). Black polygons = surface expression of volcanism; circles/triangles = loci of age-independent/-progressive whole-rock geochemical analyses; red/white fill = newly acquired/legacy data (Jones et al., 2020; O'Reilly & Zhang, 1995; Stephenson et al., 2000; Zhang et al., 2001). Inset map shows location along eastern seaboard of Australia.

son, 1989; Wellman & McDougall, 1974). Volcanic provinces are placed into these categories based upon a variety of spatial, temporal, and petrologic factors. The most subjective of these factors is whether or not volcanic provinces fit within predetermined North-South age-progressive chains of volcanoes or whether their eruption is independent of these pathways. Age-progressive activity forms chains of volcanoes that appear to track the passage of mantle plumes, such as the Cosgrove and Tasmantid chains, beneath the horizontally translating plate (Figures 1c–1e; Davies et al., 2015; Wellman & McDougall, 1974; Sutherland et al., 2012). Offshore seamount chains, central volcanoes and leucitites lie along age-progressive trends (Davies et al., 2015; Johnson, 1989).

Lava fields are defined as age-independent volcanic provinces, which consist exclusively of mafic material (Johnson, 1989; Wellman & McDougall, 1974). This age-independent activity does not obviously coincide with the passage of mantle plumes beneath the plate. Instead, it is attributed to a variety of processes that include convective upwelling at locations with steep gradients of lithospheric thickness, influx of fertile slab-derived material from subduction of the Pacific plate along the Tongan-Kermadec Trench, offshore lithospheric stretching, transtensional mantle decompression, and heat transfer from the adjacent Pacific plate mantle (Figure 1c; Demidjuk et al., 2007; Mather et al., 2020; Rawlinson et al., 2017). However, numerous lava fields are active at the same time as putative mantle plumes pass adjacent to them and so it is unclear how useful this categorization is (Figure 1c). Here, we refer to offshore seamounts, central volcanoes and leucitites as age-progressive provinces. We refer to lava fields as age-independent provinces.

Mantle plumes are vertical upwellings of hot mantle material which originate at thermal boundary layers, such as the core-mantle boundary (Morgan, 1972). When a plume reaches the base of a plate, melting can occur. Variations in melt fraction are reflected in the volume and chemical composition of mafic lavas erupted at the surface (Klein & Langmuir, 1987; McKenzie & O'Nions, 1991). Here, we characterize changes in the thermal structure of the upper mantle during Cenozoic times by exploiting the geochemical composition of these rocks. Temperature variations that we infer from analysis of volcanic rocks can be compared with independent observations. Our principal goal is to determine asthenospheric temperature and lithospheric thickness variations along the eastern seaboard of Australia and to show how this structure relates to the timing and distribution of age-progressive and age-independent volcanic provinces. Regional topography is moderated by changes in upper mantle thermal structure (Hoggard et al., 2016). In the final section, we discuss how observed mantle temperature and lithospheric thickness variations contributed to the formation of the Eastern Highlands during Late Cretaceous and Cenozoic times.

2. Upper Mantle Structure

During a field campaign to Queensland in 2017, 78 igneous rock samples were collected (Figure 2). This campaign was designed to target a combination of age-independent and age-progressive volcanic provinces where limited published geochemical information exists (e.g., Chudleigh, Sturgeon, Nebo). Samples were analyzed for major, trace and rare earth elements using XRF and ICP-MS techniques at Geoscience Australia, at the University of Cambridge, and at the University of Edinburgh (Supporting information; Data Set S2). These measurements helped to augment an extensive database of legacy geochemical measurements for eastern Australia that also includes isotopic analyses (Data Set S3; Table 1). The combined database is used to estimate potential temperature, T_p, the projected temperature that a packet of mantle has if adiabatically decompressed to surface pressures, and lithospheric thickness, a, beneath each volcanic province. By estimating T_p and a at a range of locations, spatio-temporal variations in mantle structure can be established.

Table 1
Summary of Loci, Ages and Numbers of Samples From Volcanic Provinces of Data Set S3

Province	Duration (Ma)	>6 MgO %	References
N. Queensland			
Atherton	0–7.1	8	O'Reilly and Zhang (1995); Zhang et al. (2001)
Camel Creek	~20	2	This study
Chudleigh (C)	0.24–8.98	37	Ewart et al. (1988); O'Reilly and Zhang (1995); Zhang et al. (2001, and this study).
McBride (M)	0.01–32.99	138	Ewart et al. (1988); Irving and Menzies (1991); Jones et al. (2020); Knutson (n.d.); O'Reilly and Zhang (1995); Stephenson et al. (1998); Whitehead and Stephenson (1998); Zhang et al. (2001).
Mingela	24.8–44.9	32	Knutson (n.d.); O'Reilly and Zhang (1995, and this study).
Nulla (Nu)	0–5.24	37	Ewart et al. (1988); Knutson (n.d.); O'Reilly and Zhang (1995); Stephenson et al. (2000); Zhang et al. (2001, and this study).
SPM (S)	1.2–10.8	9	Ewart et al. (1988); Zhang et al. (2001).
Sturgeon (St)	0.69–6.31	20	This study.
C. Queensland			
Bauhinia	22–28	11	Jones et al. (2020).
Buckland and Mitchell (B)	20.5–55.9	26	Crossingham et al. (2017); Ewart et al. (1988); Jones et al. (2020); Knutson (n.d.).
Monto	21–25	6	Jones et al. (2020).
Nebo (N)	14.2–54.9	61	Ewart et al. (1988); Knutson (n.d.); Sutherland (1998, 2003, and this study).
Peak Range (P)	26–47.2	82	Ewart et al. (1988); Jones et al. (2020); Knutson (n.d., and this study).
Springsure (Sp)	18.8–33.6	36	Ewart (1982); Ewart et al. (1980), (1988); Jones et al. (2020); Knutson (n.d.).
S. Queensland			
Bundaberg and Boyne	0.38–64.7	73	Ewart et al. (1988); Knutson (n.d.).
Fraser Island	19.4–30.6	3	Ewart (1982); Ewart et al. (1988).
Glass Houses	24.6–27.3	15	Ewart (1982); Ewart et al. (1988); Knutson (n.d.); Shao et al. (2015).
Main Range	18.1–34.8	151	Ewart (1982); Ewart et al. (1980), (1988); Knutson (n.d.).
Tweed	13–24.2	42	Ewart (1982); Ewart et al. (1977), (1988); Knutson (n.d.).
N. New South Wales			
Barrington	3.5–69.2	52	Jones et al. (2020); Knutson (n.d.); O'Reilly and Zhang (1995); Sutherland and Fanning (2001).
Central and Doughboy	14.2–48.7	161	Knutson (n.d.); O'Reilly and Zhang (1995); Vickery et al. (2007).
Comboyne	16.1–19.6	1	Knutson (n.d.).
Dubbo	12.2–42.7	31	O'Reilly and Zhang (1995); Sutherland (2003); Zhang and O'Reilly (1997).
El Capitan (E)	6.76–17.9	5	Nelson et al. (1986); McQueen et al. (2007).
Liverpool Range	31.78–60.4	41	Knutson (n.d.).
Nandewar	15.3–22.1	10	Knutson (n.d.); Stolz (1985).
Warrumbungle	13.7–17.4	23	Bull et al. (2020); Ghorbani and Middlemost (2000).
S. New South Wales			
Cargelligo	10.1–15.5	69	Ewart et al. (1988); Nelson et al. (1986); Knutson (n.d.).
Grabben Gullen	14–26	14	Knutson (n.d.); O'Reilly and Griffin (1984); O'Reilly and Zhang (1995).
Kandos	45–50	62	Knutson (n.d.); O'Reilly and Griffin (1984); O'Reilly and Zhang (1995).
Monaro (Mo)	29.4–55.8	38	Knutson (n.d.); Roach (1999); O'Reilly and Zhang (1995).
Oberon	17.4	16	Ewart et al. (1988); Morris (1986).
S. Highlands	28.7–43.8	111	Knutson (n.d.); Menzies and Wass (1983); O'Reilly and Zhang (1995); Wass (1980); Zhang et al. (2001).
Snowy Mountains	15.2–27.6	20	Knutson (n.d.); Sutherland et al. (2002).

Table 1
Continued

| Victoria			
Cosgrove (Co)	5.93–8.9	9	Knutson (n.d.); Nelson et al. (1986); Paul et al. (2005).
Euroa	NA	11	Paul et al. (2005).
Macedon	3.34–6.99	10	Knutson (n.d.); Paul et al. (2005).
NVP (NV)	0–7.8	492	Boyce et al. (2015); Demidjuk et al. (2007); Ellis (1976); Ewart et al. (1988); Foden et al. (2002); Frey et al. (1978); Jordan et al. (2015); Knutson (n.d.); Hare et al. (2005); McBride et al. (2001); McDonough et al. (1985); Price et al. (1991), (1997); Van Otterloo et al. (2014); Whitehead (1991).
OVP (O)	14.1–90.6	318	Frey et al. (1978); Knutson (n.d.); Price et al. (2014).
Tasmania	8–69.9	289	Adam (1990); Brown and Forsyth (1984); Brown et al. (1989); Corbett et al. (2014); Crawford et al. (1997); Everard (1989); Everard et al. (1997); Ewart et al. (1988); Knutson (n.d.); McClenaghan et al. (1982); McGee (2005); Nasir et al. (2010); Sutherland et al. (1984, 1989); Sutherland (1989a, 1989b); Sutherland et al. (1996); Sutherland (2004); Sutherland et al. (2006).

Note. Age ranges compiled from different studies (Cohen et al., 2008, 2013, 2017; Crossingham et al., 2017; 2018; Gibson, 2007; Gray & McDougall, 2009; Jones, 2018; Jones et al., 2017; Matchan & Phillips, 2014; Sutherland et al., 2012, 2014; Vasconcelos et al., 2008). Bracketed letters act as key for provinces labeled in Figure 1. Griffith (G) is labeled in Figure 1 but no samples were available for this study.
Abbreviations: NVP = Newer Volcanic Province; OVP = Older Volcanic Province; SPM = Silver Plains, Piebald and McLean.

2.1. Trace Element Modeling

Concentrations of rare earth elements (REEs) within a basaltic rock are sensitive to the conditions present when it's primary melt is generated (Gast, 1968; Kay & Gast, 1973). REEs are incompatible which means that their concentration within the melt phase reduces as melt fraction increases. Heavy REEs, such as Yb, are more compatible in garnet than light REEs, such as La. Since garnet is only present at depths that are approximately ≥63 km, REEs can be used to determine depth and temperature of melting (Jennings & Holland, 2015; Kay & Gast, 1973; McKenzie & O'Nions, 1991). If mantle composition is fixed and if melting ceases at the base of the lithosphere, depths to base and top of the melt column are predominantly controlled by T_p and a, respectively (McKenzie & Bickle, 1988). Final melt fraction is determined by the difference between these two depths. Here, we exploit the INVMEL-v12 forward model to generate a suite of REE profiles by varying T_p and a in 1°C and 1 km increments between 1,250 and 1,500°C and between 40 and 80 km, respectively (Ball et al., 2021; McKenzie & O'Nions, 1991; White & O′ Nions 1992). Averaged REE profiles from each volcanic province are compared with these modeled profiles (e.g., Figures 3a, 3c and 3e). A grid search is carried out to identify models with the smallest root mean squared (rms) misfits between calculated and average observed concentrations of La, Ce, Sm, Dy, and Yb normalized by their respective standard deviations (e.g., Figures 3b, 3d and 3f). These elements are selected because they span an appropriate range of REE partition coefficients and they are commonly measured. Models are deemed acceptable if they yield rms misfit values that are <1.5 times the misfit value of the best-fitting model.

Prior to modeling, Data Set S3 is screened in order to identify the most primitive samples from each province and thus mitigate the effects of fractional crystallisation. If possible, we exploit samples with MgO > 8.5 wt%. In provinces where <5 samples have MgO > 8.5 wt%, this MgO threshold was reduced by increments of 0.5 wt% until there are ≥5 samples with a lower limit imposed at 7 wt% of MgO. Back-calculation of olivine loss is carried out for acceptable samples until they are deemed to be in equilibrium with forsterite-90 olivine (Lee et al., 2009). Observed REE concentrations are then corrected for the amount of olivine addition, assuming that olivine contains no REEs. Note that in several instances, particularly when the MgO threshold is ≤ 8 wt%, clinopyroxene fractionation could have occurred (Jones et al., 2020). This unaccounted-for fractionation of clinopyroxene leads to an overestimate in REE concentrations for primary melts. Hence T_p values obtained by modeling samples that have experienced significant clinopyroxene fractional crystallization are necessarily underestimates.
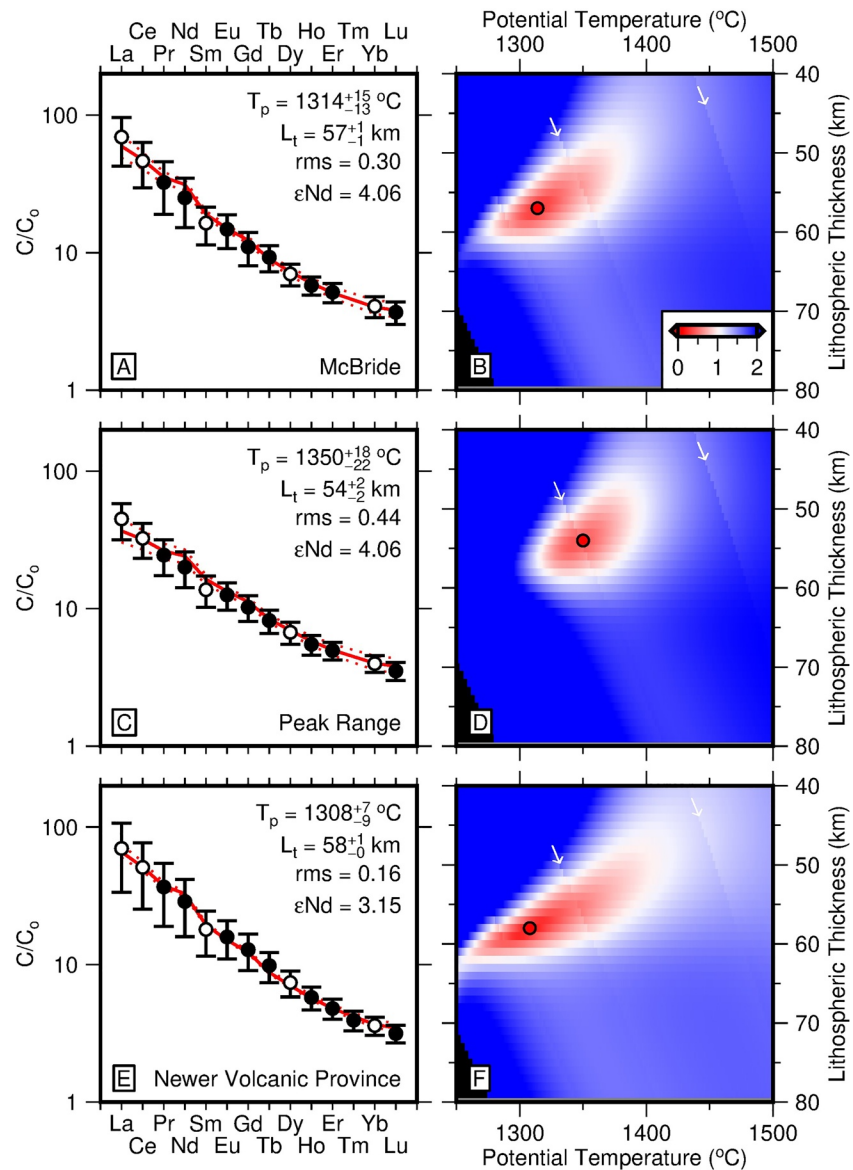
Figure 3. Inverse modeling of rare earth element (REE) concentrations. (a) McBride Province. Circles with vertical bars = average REE concentrations $\pm\sigma$ normalized with respect to source composition where $\varepsilon Nd = +4.06$; concentrations of elements with open circles used to calculate root mean squared (rms) misfit. Red line = REE concentrations calculated by inverse modeling which achieves global minimum residual rms value; pair of dotted red lines = range of calculated REE concentrations where residual rms value is 1.5× that at global minimum. Optimal values and associated uncertainties of potential temperature, T_p, of lithospheric thickness, a, residual rms value at global minimum, and of εNd are displayed at top right-hand side. (b) Misfit between observed and calculated REE concentrations plotted as function of T_p and a where color scale of rms value is given in bottom right-hand corner. Red circle = locus of global minimum of rms misfit; white arrows indicate discontinuities of rms misfit function generated by mantle phase transitions. (c) and (d) Same for Peak Range. (e) and (f) Same for the Newer Volcanic Province.

Partition coefficients for olivine, orthopyroxene and spinel required by the INVMEL-v12 algorithm are listed by McKenzie and O'Nions (1995). Coefficients for clinopyroxene and garnet are calculated using parameterizations described by Wood and Blundy (1997) and by Westrenen et al. (2001), respectively. Mineral compositions together with mantle mineralogy as a function of pressure and melt fraction are provided by McKenzie and O'Nions (1991) and by McKenzie and O'Nions (1995). We assume that the spinel-garnet transition occurs between 63 and 72 km (Klöcking et al., 2018). Source composition is calculated by matching the average εNd value for each volcanic province. This calculation is carried out using a linear mixture

of primitive and depleted peridotite mantle sources, which are assumed to have εNd values of 0 and +10, respectively (McKenzie & O'Nions, 1995). In volcanic provinces where no εNd measurements are available, the average εNd value for Cenozoic volcanic provinces of the eastern seaboard of Australia is assumed (i.e., +4.18; Table 2). The hydrous melting model of Katz et al. (2003) is used to calculate melt fraction as a function of depth for each T_p–a pair. Note that values of various parameters exploited by this melting model have been revised to honor more recent experimental constraints (Shorttle et al., 2014). Source water content is set relative to the Ce content of the source ($H_2O/Ce = 200$; Michael, 1995). Assuming that mid-oceanic ridges are underlain by depleted mantle (i.e., εNd = +10), this specific melting parameterization predicates a T_p value of 1,312°C in order to generate average oceanic crustal thickness (6.9 km; Richards et al., 2018). We assume that this value represents the ambient temperature of sub-plate mantle.

2.2. Results

Figure 3 summarizes results for three volcanic provinces: McBride, an age-independent volcanic province of Northern Queensland that has been active since ~8 Ma; Peak Range, an age-progressive volcanic province linked to the Cosgrove plume track that records volcanism between ~26 and 47 Ma; and the Newer Volcanic Province, an age-independent province in Victoria that has been active since ~6 Ma (Figure 1). In each case, an excellent fit between observed and calculated REE concentrations is obtained. Light REEs (e.g., La) typically exhibit greater standard deviations than heavy REEs (e.g., Yb). Consequently, the ratio of melting within the spinel and garnet stability fields, which principally controls heavy REE concentrations, has a greater effect upon misfit than melt fraction, which controls light REE concentrations. Therefore, a negative trade-off between T_p and a exists whereby a hotter asthenosphere but thinner plate, or a cooler asthenosphere but thicker plate, can match the observed concentrations within acceptable limits (Figure 3f). Results for individual provinces are presented in Supporting Information Figures S1–S4 and summarized in Table 2. The highest potential temperatures are recorded beneath the age-progressive provinces of central Queensland (CQ: 1348^{+28}_{-19}°C; Figure 4a). These values are ~50–100°C hotter than those values obtained for the age-independent provinces of New South Wales and Victoria (NSW and V: 1286^{+9}_{-9}°C). Temperature estimates for the age-independent volcanic provinces of Northern Queensland lie between these two extrema (NQ: 1312^{+20}_{-16}°C). Beneath the eastern seaboard of Australia, the upper boundary, at which melting ceases, is equivalent to a lithospheric thickness of 45–70 km.

T_p estimates for NSW and Victoria are up to 50°C cooler than the ambient mantle value (e.g., 1,312°C). However, the exact values of T_p and a determined using the INVMEL-v12 algorithm can change with respect to this ambient mantle value if model parameters are varied (Ball et al., 2019). For example, compositional heterogeneity of the upper mantle can influence both temperature and plate thickness. Increasing the mantle water content by 0.01 wt% shifts the value of T_p by up to +10°C and the value of a by up to −2 km. Changing mantle composition from primitive to depleted mantle decreases T_p by −20°C and increases a by +3 km. Deepening the spinel-garnet transition zone by 5 km increases T_p and a by +15°C and +5 km, respectively. The INVMEL-v12 algorithm does not take into account the presence of pyroxenitic or harzburgitic lithologies within the upper mantle. If pyroxenite or harzburgite occur within the source region, recovered values of T_p will be over- or under-estimates, respectively (Matthews et al., 2021). In summary, accurately constrained source compositions are required to improve the reliability of absolute T_p and a estimates. We acknowledge that the assumed mantle source composition is unlikely to represent the actual complexity of eastern Australian mantle. However, isotopic analyses do imply that similar mantle sources exist beneath the Cenozoic volcanic provinces of this region (Jones et al., 2020). Even though the recovered values of T_p and a have significant uncertainties, we contend that inter-provincial differences in T_p and a are robust.

Mantle melts can become enriched in incompatible elements, such as REEs, by lithospheric interactions during ascent toward the surface (Foley, 1992). Instances of contamination caused by melting of metasomatized lithospheric mantle have been reported for lavas from various Australian Cenozoic volcanic provinces (e.g., Jones et al., 2020; O'Reilly & Griffin, 1988; Shea & Foley, 2019; Zhang et al., 2001). This contamination increases REE concentrations within the melt, which causes calculated values of T_p to be underestimated (Ball et al., 2019; Klöcking et al., 2020). In locations where lithospheric contamination is reported, values of T_p should be regarded as lower estimates. In extremal cases, lithospheric contamination can enrich melts to such an extent that the INVMEL-v12 algorithm no longer successfully matches observed concentrations,

Table 2
Mantle Temperature and Lithospheric Thickness Estimates

Province	T_p (°C)	a (km)	εNd	rms	n_s	>MgO	T_p (°C)	a (km)	a (km)	a (km)
	Trace element estimate						SL2013sv		FR12	XTB
Age-independent										
Atherton	1330^{+39}_{-25}	58^{+3}_{-3}	+4.34	0.61	5	8.5	1,367	47.1	50.0	
Barrington	1264^{+25}_{-14}	60^{+3}_{-3}	+4.71	0.56	16	8.5		63	54.4	
Camel creek	1312^{+21}_{-19}	58^{+1}_{-2}	–	0.48	2	8.5		46.7	50.0	
Central	1265^{+1}_{-1}	60^{+0}_{-0}	+3.59	0.05	13	8		53.3	66.8	
Chudleigh	1312^{+27}_{-17}	60^{+1}_{-1}	+7.49	0.29	20	8.5	1,328	45.1	44.2	38
Dubbo	1318^{+6}_{-9}	55^{+1}_{-0}	0	0.12	13	8.5		74.6	69.7	
Euroa	1252^{+16}_{-0}	62^{+0}_{-2}	+2.27	0.72	10	8.5		66.6	61.6	
Grabben Gullen	1275^{+1}_{-1}	59^{+0}_{-0}	+5.28	0.08	6	8.5		75.1	40.2	
Kandos	1275^{+4}_{-3}	60^{+0}_{-0}	+3.55	0.21	13	8.5		68.7	41.2	
Liverpool range	1297^{+16}_{-15}	57^{+1}_{-2}	–	0.56	6	8.5		62.9	53.2	
McBride	1314^{+15}_{-13}	61^{+1}_{-1}	+4.06	0.30	20	8.5	1,341	47.1	50.0	53
Monaro	1278^{+4}_{-10}	58^{+1}_{-0}	+3.43	0.24	6	8.5		75.9	40.7	51
Monto	1322^{+11}_{-9}	58^{+1}_{-1}	+4.21	0.19	6	8.5		65.4	39.2	
NVP	1308^{+7}_{-9}	58^{+1}_{-0}	+3.15	0.16	72	8.5	1,298	60.9	42.7	47
Nulla	1332^{+24}_{-17}	58^{+1}_{-1}	+4.68	0.32	11	8.5	1,360	47.9	49.9	
Oberon	1304^{+19}_{-13}	59^{+1}_{-2}	–	0.26	5	8		72.4	40.3	
OVP	1296^{+17}_{-17}	57^{+1}_{-2}	+3.27	0.21	58	8.5		61.6	49.9	
Snowy mountains	1256^{+3}_{-4}	62^{+0}_{-0}	–	1.21	10	8.5		75.9	42.2	64
Southern highlands	1302^{+4}_{-3}	59^{+0}_{-0}	+2.76	0.13	8	8.5		72.4	47.5	
SPM	1256^{+4}_{-4}	65^{+2}_{-1}	+6.27	0.16	7	8.5	1,362	55.4	51.4	
Sturgeon	1325^{+12}_{-15}	58^{+1}_{-1}	–	0.32	5	8.5	1,319	67.9	72.8	
Tasmania	1278^{+5}_{-18}	60^{+2}_{-0}	+4.84	0.14	54	8.5		64.4	41.5	65
Age-progressive										
Bauhinia	1379^{+56}_{-36}	56^{+3}_{-3}	+5.11	0.62	4	8		68.9	40.2	
Buckland	1327^{+30}_{-22}	58^{+2}_{-2}	+5.92	0.75	5	8		80.3	50.0	
Nebo	1368^{+22}_{-17}	41^{+7}_{-10}	–	0.34	2	7		67.6	42.5	45
Peak Range	1350^{+18}_{-22}	54^{+2}_{-2}	+4.06	0.44	18	8.5		72.2	54.4	
Springsure	1318^{+13}_{-10}	59^{+10}_{-1}	+4.78	0.21	8	8.5		72.9	41.1	
Warrumbungle	1306^{+2}_{-2}	58^{+0}_{-0}	–	0.11	4	7.5		64.6	79.4	

Note. n_s = Number of samples; XTB = lithospheric thickness estimates from xenolith/xenocryst thermobarometry (Hoggard et al., 2020); NVP = Newer Volcanic Province; OVP = Older Volcanic Province

even for melt fractions <0.5%. For example, this inability is evident for the Cosgrove and El Capitan volcanic provinces (Figure 1a). We infer that lavas from these particular provinces could have either experienced significant lithospheric contamination, or have been sourced directly by melting of metasomatized lithosphere, which would yield extremely enriched incompatible element concentrations.

3. Comparison With Thermobarometric and Tomographic Observations

It is instructive to compare our results with estimates of T_p and a estimated by thermobarometric studies of mantle xenoliths and by analyzing calibrated seismic tomographic models. Mantle xenoliths occur in many of the Cenozoic volcanic provinces (Kay & Kay, 1983; O'Reilly & Griffin, 1985). Compositions of minerals within these xenoliths can be used to estimate the final temperatures and pressures at which xenoliths equilibrated (Nickel & Green, 1985; Nimis & Taylor, 2000). Hoggard et al. (2020) fit geothermal profiles through xenolith and xenocryst thermobarometric estimates at different locations across Australia (Figure 4c). In each case, the lithosphere-asthenosphere boundary is estimated to occur at the depth at which temperature exceeds 1,175°C. In oceanic regions, this isothermal surface coincides with a peak change in azimuthal anisotropy which demarcates the transition between conductive and convective mantle (Burgos et al., 2014; Richards et al., 2018). Values of a estimated in this way can be compared with those calculated by REE modeling (Figure 5). In each case, these estimates agree to within an average of ±12 km.

Shear-wave velocities, V_s, within the mantle are sensitive to variations in temperature, T. For a given shear-wave tomographic model, temperature structure of the mantle can be determined by calibrating the relationship between V_s and T as a function of depth. A range of global and regional tomographic models together with calculated estimates of T_p and a, exist for the Australian continent (Fishwick & Rawlinson, 2012; Hoggard et al., 2020; Kennett et al., 2013; Schaeffer & Lebedev, 2013). Here, we compare values of T_p that are calculated by REE modeling with a global mantle temperature model (Figure 4b; Hoggard et al., 2020). This particular temperature model was constructed by exploiting an empirical anelastic parameterization which describes V_s as a function of T (Richards et al., 2020; Schaeffer & Lebedev, 2013; Yamauchi & Takei, 2016). The parameterization includes unconstrained constants and it is calibrated by varying these constants to minimize the misfit between observations of mantle temperature structure and the calculated temperature model. Our chosen temperature model is underpinned by the SL2013sv tomographic model and it was principally calibrated by comparing $V_s(T)$ with an oceanic plate cooling model between depths of 0 and 125 km and to an average asthenospheric temperature profile calculated between depths of 225 and 400 km (Richards et al., 2018, 2020; Schaeffer & Lebedev, 2013; Shorttle et al., 2014).

Along the eastern seaboard of Australia, Cenozoic volcanism is focused in regions where slow shear-wave velocity anomalies and ambient or elevated temperatures lie beneath the plate. In Figure 4b, we compare tomographic estimates of T_p that are averaged between depths of 100 and 200 km with REE-modeled estimates. In order to compare these different estimates of T_p, results from each modeling approach are normalized with respect to the ambient mantle value, which yields temperature anomalies, ΔT_p. Both REE-modeled and tomographic estimates of T_p are verified by their ability to generate the average oceanic crustal thickness using an identical melting parameterization (Shorttle et al., 2014). However, the ambient value of T_p for the tomographic model is slightly higher because, in the case of the tomographic model, the mantle source is assumed to be anhydrous (1,333°C compared to 1,312°C; Ball et al., 2021; Hoggard et al., 2020; Richards et al., 2018, 2020). Since the Australian plate is rapidly translating northward at ~7 cm/yr, REE-modeled and tomographic ΔT_p estimates are only strictly comparable for the youngest volcanic provinces (<10 Ma; Northern Queensland and Newer Volcanic provinces; DeMets et al., 2010). With the exception of Silver Plains, Piebald and McLean (SPM), both ΔT_p estimates agree to within ± 20°C (Figure 4d). Note that when these techniques are applied to a global database of intraplate volcanic rocks, a systematic offset of 30–50°C is observed between REE-modeled and tomographic estimates of ΔT_p (Figure 4d; Ball et al., 2021). This offset could explain why REE-modeling estimates in NSW and Victoria are lower than ambient mantle values by ~30°C.

Changes of lithospheric thickness can also be estimated from a global temperature structure obtained for the SL2013sv model by tracking the 1,175°C isothermal surface (Hoggard et al., 2020). Lithospheric thicknesses calculated using this V_s-to-T calibration, which is based upon an oceanic plate cooling model, have
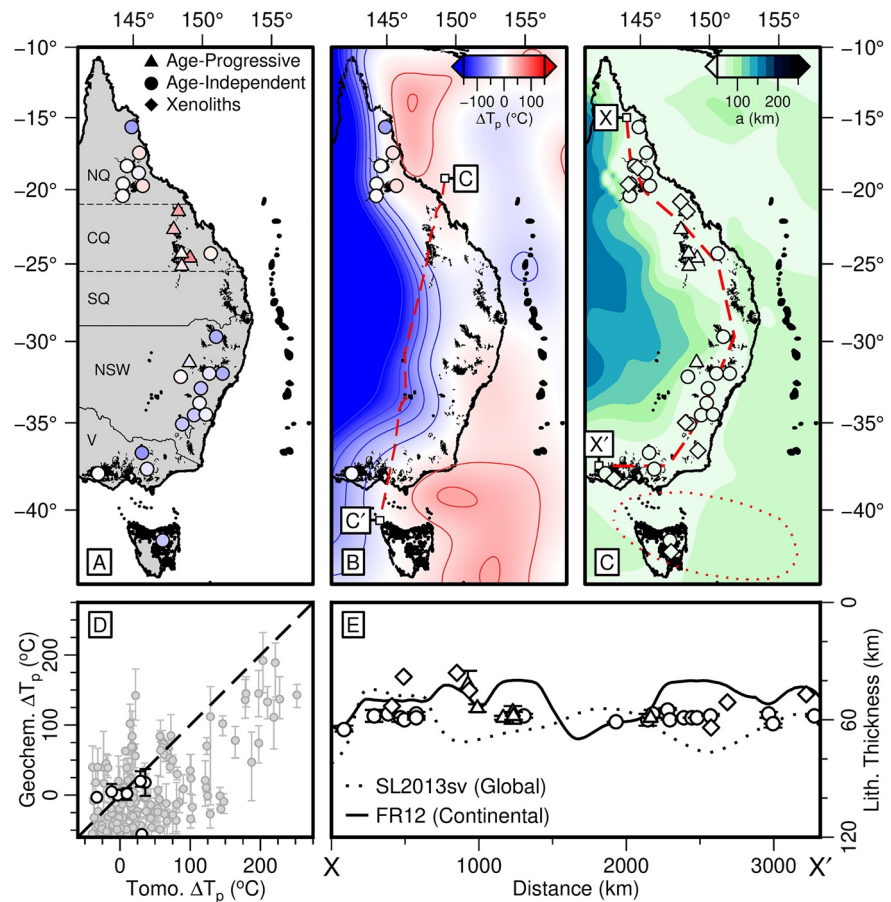
Figure 4. Mantle temperature and lithospheric thickness estimates for eastern Australia. (a) Circles/triangles = results of rare earth elements (REE) modeling for age-independent/-progressive provinces, colored by value of ΔT_p relative to 1,312°C. Black polygons = Cenozoic volcanic provinces (Raymond et al., 2012); NQ/CQ/SQ/NSW/V = Northern Queensland/Central Queensland/Southern Queensland/New South Wales/Victoria location markers. (b) Map of eastern Australia, colored by value of ΔT_p relative to 1,331°C generated from temperature-calibrated SL2013sv model averaged between 100 and 200 km (Hoggard et al., 2020; Schaeffer & Lebedev, 2013). Red/white/blue contours = positive/zero/negative ΔT_p at 25°C intervals. Circles = age-independent provinces <10 Ma colored by ΔT_p; dashed red line between C and C′ = locus of transects shown in Figure 6, which tracks relative motion of Cosgrove plume (Davies et al., 2015). (c) Lithospheric thickness calculated by tracking 1,175°C isothermal surface from temperature-calibrated FR12 model (Fishwick & Rawlinson, 2012; Hoggard et al., 2020). Diamonds = lithospheric thickness estimates constrained by xenolith/xenocryst thermobarometry (Hoggard et al., 2020). Circles/triangles = results of REE modeling colored by a. Dashed red line labeled X and X′ = locus of transect shown in panel e. (d) ΔT_p determined by REE modeling as function of ΔT_p determined by calibration of SL2013sv model. Open circles with vertical error bars = calculated values of temperature for volcanic provinces <10 Ma; dashed line = 1:1 relationship for reference; gray circles with error bars = results from equivalent global study of Neogene-Quaternary volcanic provinces (Ball et al., 2021). (e) Transect from X to X′ that intersects bulk of Cenozoic volcanic provinces. Solid/dashed line = lithospheric thickness variations determined by calibrated FR12 and SL2013sv models; symbols as before.

greater uncertainties in continental regions than in oceanic regions (Priestley & McKenzie, 2013). Since Australia is dominated by thick and depleted lithosphere, it may be more appropriate to use a lithospheric thickness model calibrated to continental temperature observations. Here, we adopt a lithospheric thickness model generated by calibrating the regional FR12 tomographic model to geothermal profiles calculated from xenolith thermobarometry (Figure 4c; Fishwick & Rawlinson, 2012; Hoggard et al., 2020). This regional lithospheric thickness model predicts thinner lithosphere beneath cratonic Australia compared with the global model. In areas of thin lithosphere relevant to our study, these models broadly agree. Both regional and global tomographic estimates of a are consistent with geochemical estimates within an average
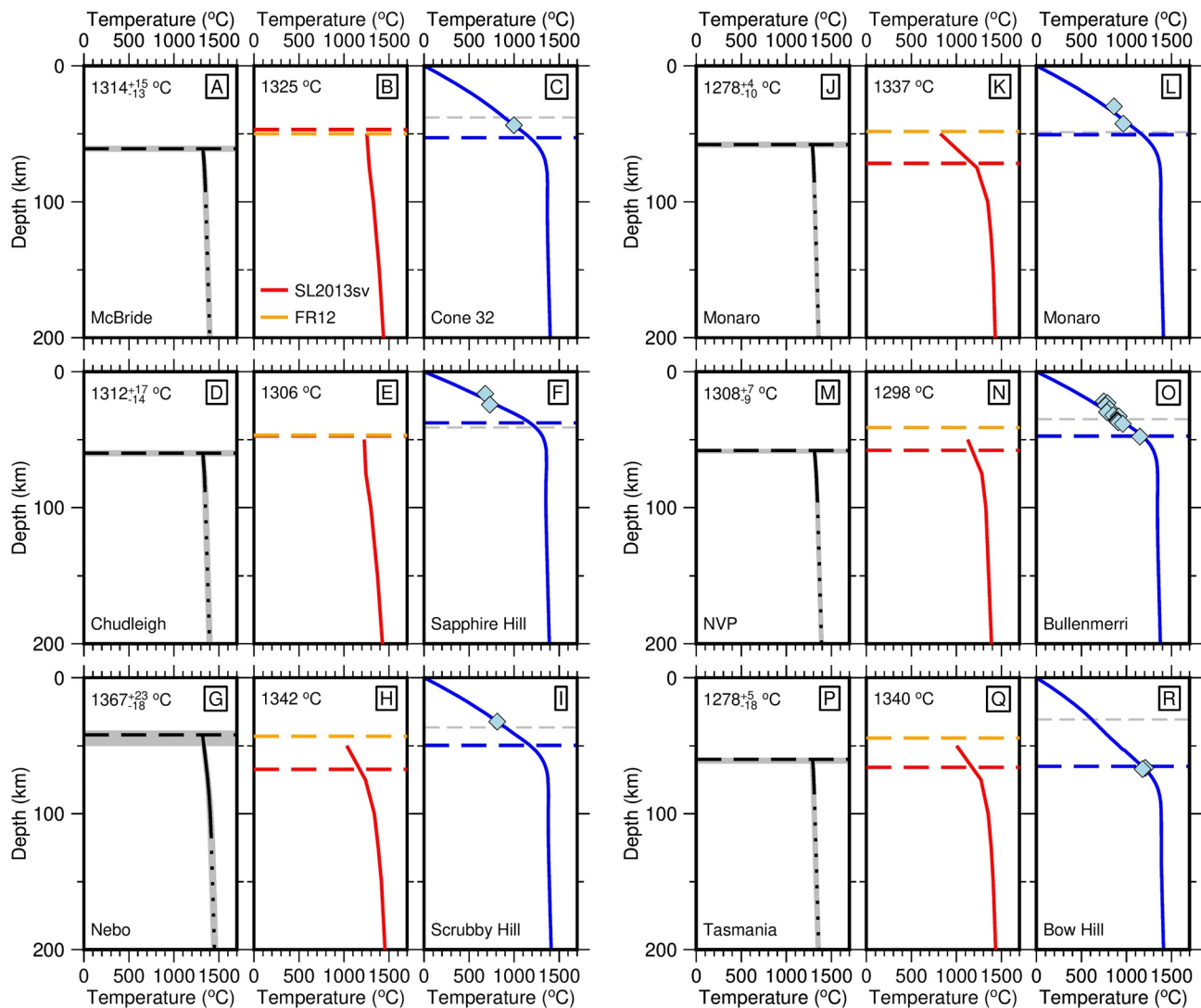
Figure 5. Comparisons between geochemical and geophysical predictions of upper mantle structure. (a) Temperature structure beneath McBride province calculated by modeling REE concentrations of mafic rocks. Dotted line = temperature as function of depth at subsolidus conditions for optimal melting model; solid line = temperature as function of depth within melting region; horizontal dashed line = predicted lithospheric thickness for optimal model; gray bars = uncertainties for estimates of T_p and a. Best-fitting potential temperature shown in top left-hand corner. (b) Shear-wave-velocity-to-temperature conversion (Hoggard et al., 2020). Solid red line = temperature as function of depth beneath McBride calculated from SL2013sv model; dashed red/orange line = lithospheric thickness predicted by 1,175°C isothermal surface from SL2013sv/FR12 models. Average potential temperature between 100 and 200 km for SL2013sv model shown in top left-hand corner. (c) Paleogeothermal profile calculated using xenoliths/xenocrysts from Cone 32, McBride. Blue diamonds = xenolith/xenocryst thermobarometric estimates (Hoggard et al., 2020); dashed gray line = crustal thickness from AusMoho compilation (Kennett et al., 2011); solid line = optimal paleogeothermal profiles, calculated from thermobarometric and crustal thickness constraints using FITPLOT algorithm and estimate of T_p from geochemical modeling (Hoggard et al., 2020; Kay & Kay, 1983; Mather et al., 2011; McKenzie et al., 2005; Stolz, 1987); dashed blue line = lithospheric thickness defined by intersection of palaeogeothermal profile with 1,175 °C isothermal surface. (d)–(f) Same for Chudleigh volcanic province, which contains Sapphire Hill xenolith/xenocryst location (Kay & Kay, 1983). (g)–(i) Same for Nebo volcanic province, which contains Scrubby Hill xenolith/xenocryst location (Griffin et al., 1987). (j)–(l) Same for Monaro volcanic province and xenolith/xenocryst location (Roach, 2004). (m)–(o) Same for Newer Volcanic Province (NVP), which contains Bullenmerri Maar xenolith/xenocryst location (Griffin et al., 1984). (p)–(r) Tasmania volcanic province, which contains Bow Hill xenolith/xenocryst location (Sutherland et al., 1984).

of ±12 km along the length of the eastern seaboard (Figure 4e). Therefore, seismic tomographic models provide a useful means of extrapolating lithospheric thickness between point-wise xenolith thermobarometric constraints. Tomographic estimates of a are <80 km for all volcanic provinces, with the exception of the east Australian leucitites (e.g., El Capitan (E), Griffith (G), Cosgrove (Co); Figure 1a). Elevated REE concentrations indicative of lithospheric contamination reported for Cosgrove and El Capitan, coupled with a lack of

xenolith thermobarometric observations, mean that these tomographic estimates of lithospheric thickness cannot be geochemically corroborated.

4. Mechanisms for Generating Cenozoic Volcanism

All three techniques used to estimate upper mantle structure along the eastern seaboard of Australia are subject to significant uncertainties. Nevertheless, the self-consistency of our results is notable, which supports the inference that chemical composition of Cenozoic volcanic rocks is a function of upper mantle conditions at the time of melt generation. Here, we discuss potential mechanisms for generating both age-progressive and age-independent volcanism in this region.

The REE modeling results presented here include the first attempt to estimate the temperature of the putative Cosgrove mantle plume. To reproduce REE concentrations of the Central Queensland age-progressive volcanic rocks, potential temperatures, that are ~50–100°C hotter than those needed to produce age-independent volcanism of New South Wales, are required. Assuming that age-independent volcanism of NSW was generated at ambient mantle temperatures, we estimate that the Cosgrove plume had an excess temperature of 50–100°C when Central Queensland translated over it. REE concentrations and absolute temperatures estimated for Central Queensland are similar to those calculated using the same techniques applied to the present-day Réunion mantle plume (Ball et al., 2021). These temperatures are amongst the hottest recorded on Earth during Neogene-Quaternary times using this modeling scheme (Ball et al., 2021).

The Older and Newer Volcanic provinces are geographically proximal to one another within the state of Victoria (Figure 1a). The Older Volcanic Province (OVP) was active between ~90 and 14 Ma, whilst the Newer Volcanic Province (NVP) has been active since ~6 Ma (Gray & McDougall, 2009; Price et al., 2014). Volcanic activity of the NVP is coincident with passage of the Cosgrove mantle plume beneath Victoria (Davies et al., 2015). Since, at the time of eruption, the Cosgrove plume was present beneath the NVP and absent beneath the OVP, we would expect to see a difference in T_p estimates between these provinces. However, we obtain similar T_p results in both cases, which indicates that the plume may have thermally waned by the time it passed beneath Victoria (1296^{+11}_{-13}°C and 1308^{+4}_{-3}°C, respectively; Figure 6a). Significantly, a discrete low velocity anomaly at the predicted location of the present-day plume head is generally absent from tomographic models (C′ in Figure 4b). We note, however, that recent seismic imaging using observations from the WOMBAT and BASS arrays, reveals radial anisotropy that could be generated by radial flow away from a plume conduit (Bello et al., 2019).

The Eastern Australian leucitites are also thought to have been generated by passage of the Cosgrove mantle plume (Davies et al., 2015). These K-rich, leucite-bearing lava flows crop out between Central Queensland and the Newer Volcanic Province (e.g., El Capitan, Griffith, Cosgrove volcanic provinces; Figure 1a). Using either global or regional tomographic models, this area is predicted to have lithosphere >100–200 km thick (Figure 6b). Thick lithosphere largely inhibits melting and so, based upon these models, no magmatism would be expected to occur beneath regions where leucitites crop out. However, a regional P-wave tomographic model based upon observations from the WOMBAT array, which is positioned south of ~29°S, suggests that these low-volume leucititic melts could form over localized regions of thin lithosphere that cannot be resolved by large-scale tomographic models (Davies et al., 2015). Unfortunately, regional tomographic models are difficult to calibrate with a view to extracting temperature and lithospheric structure. Nonetheless, we can estimate values of lithospheric thickness from the WOMBAT-based model by assuming that minimum and maximum P-wave velocities along the Cosgrove track coincide with the thinnest and thickest lithosphere, respectively (Davies et al., 2015). By linearly scaling P-wave velocities with respect to values of lithospheric thickness between these extreme values, regions of lithosphere <80 km thick are predicted to occur beneath all leucitite outcrops (Figure 6b). In these regions, the lithosphere is sufficiently thin to permit small degrees of partial melting (Figure 6c). Note that, if the leucitites are formed by melting of metasomatized lithosphere, which is a reasonable conclusion given their K-rich composition, elevated asthenospheric temperatures are required to initiate melting and to form age-progressive volcanism.

Although our results suggest thermal waning of the Cosgrove plume, we cannot constrain its timing. Mapping of volcanic provinces across Central Queensland reveals a southward decrease in melt volume,
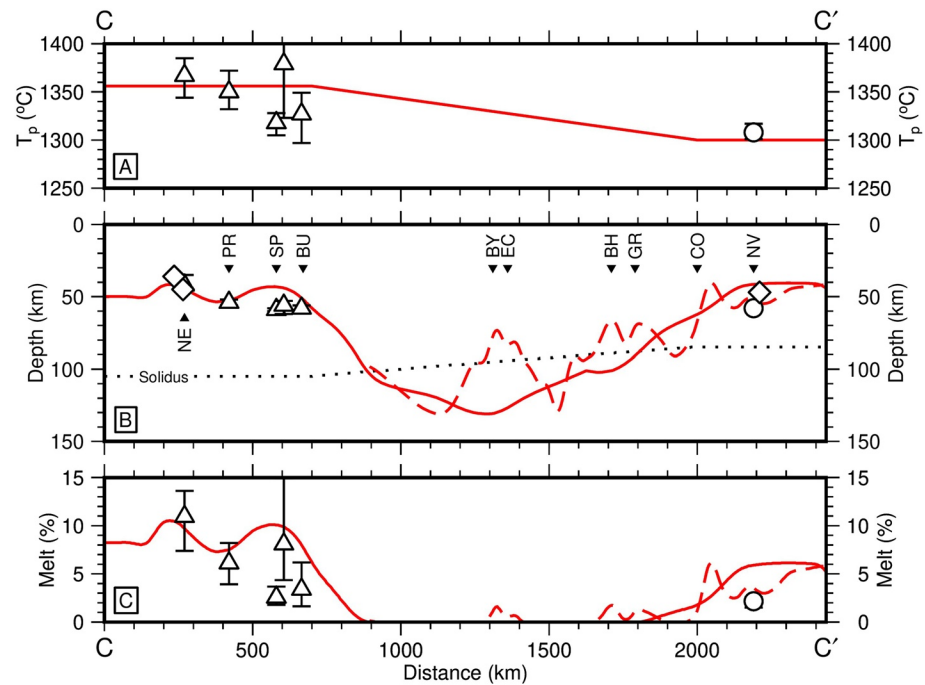
Figure 6. North-South transect from C to C' in Figure 4b which tracks the Cosgrove plume (Davies et al., 2015). (a) Temperature profile of Cosgrove plume estimated using results of geochemical modeling. Circles/triangles = age-independent/-progressive estimates of T_p from rare earth element (REE) modeling; red line = estimated temperature profile for the Cosgrove plume. (b) Red solid/dashed lines = estimates for lithospheric thickness from FR12/FR12 modified by linearly scaling lithospheric thickness using average P-wave velocities over depth range of 50–200 km from WOMBAT database (Davies & Rawlinson, 2014; Hoggard et al., 2020); circles/triangle/diamonds = age-independent/-progressive/xenolith thermobarometric estimates of lithospheric thickness; dotted line = depth of solidus, assuming that mantle H_2O concentration = 210 ppm (Shorttle et al., 2014); NE = Nebo; PR = Peak Range; SP = Springsure; BU = Buckland; BY = Byrock; EC = El Capitan; BH = Begargo Hill; GR = Griffith; NV = New Volcanic Province. (c) Red solid/dashed lines = melt fraction estimates obtained by assuming adiabatic upwelling to base of lithosphere from FR12 and modified FR12 models (Shorttle et al., 2014); circles/triangles = age-independent/-progressive melt fraction estimates.

which is attributed to a waning plume (Jones et al., 2017). In this region, it is likely that lithospheric thickness increases southward since volcanic activity occurs closer to the thick cratonic interior (Figure 4c). Therefore, a reduction of melt volume within Central Queensland could, instead, be due to the plume beginning to track beneath thicker lithosphere (Davies et al., 2015). However, exploiting current tomography-based lithospheric thickness models, a pronounced increase in lithospheric thickness is not observed until south of the Central Queensland volcanic provinces, and lithospheric thickness variations cannot account for T_p differences between Central Queensland and Victoria (Figure 6; Hoggard et al., 2020). Gradual, rapid, or even delayed, thermal waning of the Cosgrove plume between Central Queensland and Victoria can each account for formation of all volcanic provinces along the plume track (Figure S5). Unfortunately, a paucity of REE compositions for age-progressive volcanism in Southern Queensland, for NSW, and for the offshore seamounts limits the spatial coverage of our study. Further analysis of mafic rocks from age-progressive volcanic provinces would be helpful to constrain in more detail the number, location and temperature excess of mantle plumes that have passed beneath Australia during Cenozoic times.

Results of REE modeling suggest that generation of age-independent volcanic provinces across NSW requires a combination of either ambient or modestly elevated asthenospheric temperatures and thinned lithosphere. This combination could be consistent with the hypothesis that age-independent volcanism is generated by either edge-driven convection and/or shear-driven upwelling of mantle material. In this hypothesis, the juxtaposition of thick cratonic lithosphere with thinner coastal lithosphere facilitates generation of local edge-driven convective cells that sustain intermittent volcanic activity over protracted periods

of time (Davies & Rawlinson, 2014; Demidjuk et al., 2007; Rawlinson et al., 2017). Rapid northward translation of Australia could modify the flow field in the mantle beneath, initiating shear-driven upwelling and altering the distribution and extent of volcanic activity at the surface (Davies & Rawlinson, 2014; Rawlinson et al., 2017). Since eruptions have not been continuous throughout Cenozoic times, it is possible that minor variations of mantle temperature, lithospheric structure, mantle flow and/or asthenospheric composition act to modulate the melting process (Demidjuk et al., 2007; Mather et al., 2020; Rawlinson et al., 2017).

Our REE modeling results suggest that ambient to modestly elevated asthenospheric potential temperatures exist at the present day beneath Northern Queensland. These results are corroborated by seismic tomographic estimates of T_p (Figures 4b and 4d). As such, it is unlikely that age-independent volcanism of Northern Queensland and NSW are generated by identical processes. Northern Queensland lies at the leading edge of the translating Australian plate, which is a dynamically unfavorable locus for melting to have occurred either by edge-driven convection or by shear-driven upwelling (Davies & Rawlinson, 2014; Rawlinson et al., 2017). Instead, intraplate volcanism of Northern Queensland could have been generated by the recent arrival of a mantle plume (Kennett & Davies, 2020). Beneath the Coral Sea, a deep-rooted plume is inferred to exist within the lower mantle that has associated seismic attenuation within the upper mantle (French & Romanowicz, 2015; Kennett & Davies, 2020). However, no bathymetric swell is observed at the predicted location of this plume. Instead, a significant negative residual depth anomaly is recorded throughout the Coral Sea where stratigraphic evidence suggests that this subsidence occured during Neogene times (Czarnota et al., 2013; Hoggard et al., 2017; Müller, Gaina, & Clark, 2000). Absence of a clearly defined plume within the upper mantle, combined with the geographic distribution of volcanism, could result from interaction between a rising plume and subducted oceanic lithosphere within the mid-mantle (Kennett & Davies, 2020). Further investigation is required to determine the mechanism that generates the volcanism of Northern Queensland, although the modestly elevated temperatures estimated by REE modeling are indeed compatible with the presence of a mantle plume.

5. Evolution of the Eastern Highlands

We have used a database of newly acquired and legacy geochemical measurements to constrain values of T_p and lithospheric thickness beneath the eastern seaboard of Australia. Our results agree to within an average of ±20°C and ±12 km of tomographic and xenolith thermobarometric estimates. They show that lithosphere beneath the eastern seaboard is < 80 km thick throughout Cenozoic times. This thin lithosphere is underlain by asthenospheric mantle whose potential temperature varies as a function of time and space. The bulk of Cenozoic volcanism occurs within the Eastern Highlands, which sit at present-day elevations of 500–1,500 m. Here, we explore the geodynamical implications of our results. We suggest that a combination of lithospheric thinning and asthenospheric flow could be responsible for the formation and longevity of the Eastern Highlands.

To assess the upper mantle's contribution to formation of the Eastern Highlands, we must first constrain the timing and extent of uplift. In Northern Queensland, Late Cretaceous marine sedimentary rocks capped by lateritic deposits are distributed along the western edge of these highlands (Coventry et al., 1985; Wellman, 1987). Laterite deposits build up during prolonged spells of sub-aerial weathering in hot tropical environments where topographic gradients are minimal. These combined stratigraphic and geomorphic observations suggest that sub-aerial exposure of Northern Queensland occurred between 100 and 45 Ma (Wellman, 1979, 1987). We infer that Cenozoic volcanism occurred onshore and commenced when topographic relief was low.

To the south, post-Triassic marine sedimentary rocks are absent which means that the commencement of sub-aerial exposure is poorly constrained. Within the Monaro volcanic province, basaltic lavas that erupted at ~45 Ma flowed along deeply incised paleovalleys, which implies that a component of regional topography existed during Mesozoic times (Taylor et al., 1985; Vandenberg, 2010). Forward and inverse modeling of longitudinal river profiles from the Eastern Highlands reveals a two phase uplift history (Czarnota et al., 2014; Salles et al., 2017). Within the southeastern highlands, where erosion rates are best-constrained, these phases occurred in Late Cretaceous (i.e., 120–80 Ma) and Cenozoic (i.e., 60–30 Ma) times, respectively (Czarnota et al., 2014; Young & McDougall, 1993). Apatite (U−Th)/He thermochronologic analyses of sedimentary

rocks from the Drummond basin of southern Queensland suggest that cooling and exhumation of this basin began at ~90 Ma (Zhang et al., 2019). A subsequent period of Cenozoic uplift and denudation is consistent with other geomorphologic, fission track and stratigraphic studies (Faiz et al., 2007; Holdgate et al., 2008; O'Sullivan et al., 1995, 2000; Wellman, 1987). This second phase of regional uplift coincides with onset of intraplate volcanism. Sub-aerial lava flows with radiometric dates of ~30 Ma crop out at elevations of ~30 m along the coastline adjacent to the southeastern and central highlands (Young & McDougall, 1982; Young & Wray, 2000). These flows demonstrate that most of the regional uplift occurred prior to Oligocene times. Although this two phase uplift model for the Eastern Highlands is widely accepted, the relative contributions of each uplift phase to present-day topography remains debated (Czarnota et al., 2014; Hill, 1999; Holdgate et al., 2008; Salles et al., 2017; Vandenberg, 2010; Webb, 2017).

Some previous studies have attributed regional uplift of the Eastern Highlands to crustal, rather than mantle, processes. These processes include tectonic shortening, rifting during opening of the Tasman Sea, magmatic underplating, and erosion of pre-existing topography (Holdgate et al., 2008; Kohn et al., 2002; Lister & Etheridge, 1989; Stephenson & Lambeck, 1985; Van der Beek et al., 1999). These alternative proposals generally assume that present-day topography is supported by crustal thickness and density variations. For example, in the southernmost Eastern Highlands, topography does indeed correlate with crustal thickness and with present-day seismic activity. Therefore, on local scales, this assumption may hold (Braun et al., 2009; Kennett et al., 2011; Sandiford et al., 2004). Models of the SE Australian stress regime indicate that an E-W compressive stress field developed at 5–10 Ma (Sandiford et al., 2004). Crustal shortening attributable to these stresses could account for a small proportion (i.e., < 200 m) of uplift during or after the second phase of Eastern Highlands formation (Braun et al., 2009). However, the Eastern Highlands coincide with positive long wavelength free-air gravity anomalies (Figure 1a). Thus it is less likely that the whole of the Eastern Highlands is supported by crustal isostasy alone. Instead, admittance analysis of eastern Australia implies that a combination of mantle density variations and normal stresses, probably generated by asthenospheric flow, support the Eastern Highlands (Czarnota et al., 2014).

It is unlikely that the Eastern Highlands have been consistently supported by thermally buoyant asthenosphere since our geochemical analyses suggest that the generation of age-independent volcanism does not require excess mantle temperatures. Rapid northward translation of the Australian plate during Cenozoic times also negates this possibility. Numerous studies have advocated lower mantle density variations as a key control of eastern Australian topography. Regional uplift of the Eastern Highlands could conceivably be produced by migration of the Australian continent away from a sinking slab within the mantle and toward the Pacific Large Low Velocity Province (Gurnis et al., 1998; Müller et al., 2016; Salles et al., 2017). The predicted surface rebound of ~1,000 m generated by lateral motion over these deep mantle features encompasses both the Eastern Highlands together with the Coral and Tasman seas, which lie to the east. In contrast to the Eastern Highlands, the Tasman and Coral seas are associated with negative long wavelength free-air gravity anomalies, negative residual topography, and hundreds of meters of Neogene-Quaternary subsidence (Figure 1a; Czarnota et al., 2013; Müller, Lim, & Isern, 2000). Accordingly, whilst this hypothesis can match the magnitude and timing of uplift observed for the Eastern Highlands, it is difficult to reconcile it with proximal offshore observations. Finally, modest predictions of dynamic topographic support at the present day (i.e., −100 m to +200 m) are at odds with the existence of a positive free-air gravity anomaly and with the requirement for sub-crustal support across the Eastern Highlands (Czarnota et al., 2014). These observations imply that additional processes are necessary to generate and maintain both the Eastern Highlands and the dynamic topographic low of the Coral and Tasman seas.

An alternative (or additional) mechanism for generating regional uplift is thinning of lithospheric mantle (Bird, 1979). Our results show that the lithosphere beneath the eastern seaboard of Australia was thin prior to, or coincident with, onset of volcanism. Thin lithosphere persists to the present day. Using a simple isostatic calculation, thinning of lithosphere from 120 to 70 km by removal of lithospheric mantle material will generate either 0.72 km or 1.26 km of regional uplift, depending upon whether the remnant lithosphere is thermally dis-equilibrated or re-equilibrated (Appendix A). Therefore, lithospheric erosion can provide sufficient buoyancy to support the Eastern Highlands, which have a present-day elevation of 0.5–1.5 km. Any hypothesis that accounts for support of the Eastern Highlands must reproduce its two phase uplift history (Czarnota et al., 2014; Müller et al., 2016; Salles et al., 2017). These highlands could initially have been

uplifted by erosion of lithospheric mantle prior to the opening of the Southern ocean and of the Tasman sea at ~90 Ma (Gaina et al., 1998). The second phase of uplift coincides with onset of volcanism and with an increase in plate speed as the Australian plate begins to separate from Antarctica and translate toward the Melanesian subduction zone at 60–30 Ma (DeMets et al., 2010; Müller, Gaina, & Clark, 2000). Along the eastern seaboard of Australia, thin coastal lithosphere abuts the thick cratonic interior at the present day (Figure 4c). As plate speed increases, local convection cells that develop at marked changes in lithospheric thickness are conceivably enhanced (Conrad et al., 2010; Davies & Rawlinson, 2014; Rawlinson et al., 2017). These putative cells could destabilize overlying lithospheric mantle and could also contribute hundreds of meters of dynamic support at wavelengths of order 10^2–10^3 km, as a consequence of normal stresses imparted by shallow mantle flow (Colli et al., 2016; Kim & So, 2020). Return convective flow could also generate observed subsidence of the Coral and Tasman seas. The surprising longevity of thinned lithosphere along the eastern seaboard and, therefore, of the Eastern Highlands, could result from some combination of shear-driven upwelling, edge-driven convection and/or periodic small-scale melting, which act to inhibit lithospheric rethickening.

6. Conclusions

A revised and augmented geochemical database of Cenozoic volcanism along the eastern seaboard of Australia has been compiled and analyzed. This database includes newly acquired samples and analyses from a series of under-represented locations across Queensland. Geochemical modeling of this database suggests that continental lithosphere is < 80 km thick and that ambient, or modestly elevated, mantle temperatures existed beneath age-independent volcanic provinces during Cenozoic times. Both thinning of the lithospheric mantle and development of small-scale convection cells within the uppermost asthenosphere prior to, or coincident with, the onset of volcanism could have contributed to regional uplift of the Eastern Highlands. Excess mantle temperatures of 50–100°C are required to produce the age-progressive volcanic provinces of Central Queensland. These excess temperatures mark the passage of the Cosgrove mantle plume beneath the horizontally translating plate. We observe a thermal waning of this plume as it passes beneath the plate. Results of modeling of REE concentrations agree with independent constraints obtained from xenolith thermobarometric and seismic tomographic analyses, which validates our proposed lithospheric architecture. In the future, quantitative geochemical modeling of older volcanic provinces should yield useful insights into the way in which mantle structure of the Australian plate has evolved through geologic time.

Appendix A: Isostatic Calculations

The amount of regional uplift, U, generated by removal of dense lithospheric mantle is given by

$$U = (z_{l,o} - z_c)\frac{\rho_{lm,o}}{\rho_a} - (z_{l,n} - z_c)\frac{\rho_{lm,n}}{\rho_a} - (z_{l,o} - z_{l,n}), \tag{A1}$$

where z and ρ refer to thicknesses and densities, respectively. Subscript labels are as follows: c indicates crust; l indicates lithosphere; lm indicates lithospheric mantle; and a indicates asthenosphere. Subscripts o and n refer to original and modified lithospheric columns, respectively. Lithospheric and asthenospheric densities are functions of pressure and temperature. Here, we use identical equations and parameter values to those described by Ball et al. (2019). We assume $T_p = 1{,}330$°C, an asthenospheric temperature gradient of 0.6°C km^{-1}, a pressure gradient of 0.033 GPa km^{-1}, a reference mantle density of 3.33 Mg m^{-3}, a thermal expansion coefficient of 4×10^{-5} °C^{-1}, and a bulk modulus of 115.2 GPa. In the thermally equilibrated case, the base the of lithospheric column is assumed to have a T_p of 1,330°C with temperature that linearly decreases to zero at Earth's surface. In the disequilibrated case, temperature profile remains fixed so that the base of the lithosphere has $T_p < 1{,}330$°C and temperature linearly decreases to zero at the Earth's surface. For these calculations, we assume that $z_c = 35$ km and that the lithosphere is not depleted. If lithosphere with a thickness of 120 km is instantaneously thinned to 70 km, $U = 0.72$ km. If this perturbed lithospheric column is thermally re-equilibrated, it becomes less dense and U increases to 1.25 km. The effects of mantle flow and regional denudation can act to amplify U.

Data Availability Statement

Newly acquired analyses are provided in Supporting information, through Geoscience Australia and in the EarthChem data repository (https://doi.org/10.26022/IEDA/111889). INVMEL-v12 software was developed and is owned by D. McKenzie to whom requests for access should be directed. For access to other software please contact authors.

References

Adam, J. (1990). The geochemistry and experimental petrology of sodic alkaline basalts from Oatlands, Tasmania. *Journal of Petrology*, *31*(6), 1201–1223. https://doi.org/10.1093/petrology/31.6.1201

Ball, P. W., White, N. J., Maclennan, J., & Stevenson, S. N. (2021). Global influence of mantle temperature and plate thickness on intraplate volcanism. *Nature Communications*, *12*(2045), 1–13. https://doi.org/10.1038/s41467-021-22323-9

Ball, P. W., White, N. J., Masoud, A., Nixon, S., Hoggard, M., Maclennan, J., et al. (2019). Quantifying asthenospheric and lithospheric controls on mafic magmatism across North Africa. *Geochemistry, Geophysics, Geosystems*, *20*, 3520–3555. https://doi.org/10.1029/2019gc008303

Bello, M., Cornwell, D., Rawlinson, N., & Reading, A. (2019). Insights into the structure and dynamics of the upper mantle beneath Bass Strait, southeast Australia, using shear wave splitting. *Physics of the Earth and Planetary Interiors*, *289*, 45–62. https://doi.org/10.1016/j.pepi.2019.02.002

Bird, P. (1979). Continental delamination and the Colorado Plateau. *Journal of Geophysical Research*, *84*(B13), 7561–7571. https://doi.org/10.1029/jb084ib13p07561

Boyce, J. A., Nicholls, I. A., Keays, R. R., & Hayman, P. C. (2015). Variation in parental magmas of Mt Rouse, a complex polymagmatic monogenetic volcano in the basaltic intraplate newer Volcanics Province, southeast Australia. *Contributions to Mineralogy and Petrology*, *169*(2), 11. https://doi.org/10.1007/s00410-015-1106-y

Braun, J., Burbidge, D., Gesto, F., Sandiford, M., Gleadow, A. J. W., Kohn, B., & Cummins, P. (2009). Constraints on the current rate of deformation and surface uplift of the Australian continent from a new seismic database and low-T thermochronological data. *Australian Journal of Earth Sciences*, *56*(2), 99–110. https://doi.org/10.1080/08120090802546977

Brown, A., McClenaghan, M., Turner, N., Baillie, P., McClenaghan, J., & Calver, C. (1989). *Geological atlas 1: 50 000 series. Sheet 73 (8112N). Huntley (tech. rep.)*. Geological Survey of Tasmania.

Brown, A. V., & Forsyth, S. M. (1984). Chemistry of tertiary basalt and palynology of interbedded sediments from B.H.P drill holes (Vol. 39). Tasmanian Department of Mines.

Bruinsma, S. L., Förste, C., Abrikosov, O., Lemoine, J.-M., Marty, J.-C., Mulet, S., et al. (2014). ESA's satellite-only gravity field model via the direct approach based on all GOCE data. *Geophysical Research Letters*, *41*(21), 7508–7514. https://doi.org/10.1002/2014gl062045

Bull, K., Troedson, A., Bodorkos, S., Blevin, P., Bruce, M., & Waltenberg, K. (2020). Warrumbungle Volcano: Facies architecture and evolution of a complex shield volcano. *Australian Journal of Earth Sciences*, 1–39. https://doi.org/10.1080/08120099.2020.1764622

Burgos, G., Montagner, J.-P., Beucler, E., Capdeville, Y., Mocquet, A., & Drilleau, M. (2014). Oceanic lithosphere-asthenosphere boundary from surface wave dispersion data. *Journal of Geophysical Research: Solid Earth*, *119*(2), 1079–1093. https://doi.org/10.1002/2013jb010528

Cohen, B. E., Knesel, K. M., Vasconcelos, P. M., & Schellart, W. P. (2013). Tracking the Australian plate motion through the Cenozoic: Constraints from 40Ar/39Ar geochronology. *Tectonics*, *32*(5), 1371–1383. https://doi.org/10.1002/tect.20084

Cohen, B. E., Knesel, K. M., Vasconcelos, P. M., Thiede, D. S., & Hergt, J. M. (2008). ^{40}Ar/^{39}Ar constraints on the timing and origin of Miocene leucitite volcanism in southeastern Australia. *Australian Journal of Earth Sciences*, *55*(3), 407–418. https://doi.org/10.1080/08120090701769514

Cohen, B. E., Mark, D. F., Fallon, S. J., & Stephenson, P. J. (2017). Holocene-Neogene volcanism in northeastern Australia: Chronology and eruption history. *Quaternary Geochronology*, *39*, 79–91. https://doi.org/10.1016/j.quageo.2017.01.003

Colli, L., Ghelichkhan, S., & Bunge, H.-P. (2016). On the ratio of dynamic topography and gravity anomalies in a dynamic Earth. *Geophysical Research Letters*, *43*(6), 2510–2516. https://doi.org/10.1002/2016GL067929

Conrad, C. P., Wu, B., Smith, E. I., Bianco, T. A., & Tibbetts, A. (2010). Shear-driven upwelling induced by lateral viscosity variations and asthenospheric shear: A mechanism for intraplate volcanism. *Physics of the Earth and Planetary Interiors*, *178*(3–4), 162–175. https://doi.org/10.1016/j.pepi.2009.10.001

Corbett, K., Quilty, P., & Calver, C. (2014). Geological evolution of Tasmania (Vol. 24). Geological Society of Australia - Tasmanian Division.

Coventry, R., Stephenson, P., & Webb, A. (1985). Chronology of landscape evolution and soil development in the upper Flinders River area, Queensland, based on isotopic dating of Cainozoic basalts. *Australian Journal of Earth Sciences*, *32*(4), 433–447. https://doi.org/10.1080/08120098508729342

Crawford, A. J., Lanyon, R., Elmes, M., & Eggins, S. (1997). Geochemistry and significance of basaltic rocks dredged from the South Tasman Rise and adjacent seamounts. *Australian Journal of Earth Sciences*, *44*(5), 621–632. https://doi.org/10.1080/08120099708728341

Crossingham, T. J., Ubide, T., Vasconcelos, P. M., Knesel, K. M., & Mallmann, G. (2018). Temporal constraints on magma generation and differentiation in a continental volcano: Buckland, eastern Australia. *Lithos*, *302–303*, 341–358. https://doi.org/10.1016/j.lithos.2018.01.009

Crossingham, T. J., Vasconcelos, P. M., Cunningham, T., & Knesel, K. M. (2017). 40Ar/39Ar geochronology and volume estimates of the Tasmantid Seamounts: Support for a change in the motion of the Australian plate. *Journal of Volcanology and Geothermal Research*, *343*, 95–108. https://doi.org/10.1016/j.jvolgeores.2017.06.014

Czarnota, K., Hoggard, M., White, N., & Winterbourne, J. (2013). Spatial and temporal patterns of Cenozoic dynamic topography around Australia. *Geochemistry, Geophysics, Geosystems*, *14*(3), 634–658. https://doi.org/10.1029/2012gc004392

Czarnota, K., Roberts, G., White, N., & Fishwick, S. (2014). Spatial and temporal patterns of Australian dynamic topography from river profile modeling. *Journal of Geophysical Research: Solid Earth*, *119*, 1384–1424. https://doi.org/10.1002/2013JB010436

Davies, D. R., & Rawlinson, N. (2014). On the origin of recent intraplate volcanism in Australia. *Geology*, *42*(12), 1031–1034. https://doi.org/10.1130/g36093.1

Davies, D. R., Rawlinson, N., Iaffaldano, G., & Campbell, I. (2015). Lithospheric controls on magma composition along Earth's longest continental hotspot track. *Nature*, *525*(7570), 511, 514. https://doi.org/10.1038/nature14903

DeMets, C., Gordon, R. G., & Argus, D. F. (2010). Geologically current plate motions. *Geophysical Journal International*, *181*(1), 1–80. https://doi.org/10.1111/j.1365-246x.2009.04491.x

Demidjuk, Z., Turner, S., Sandiford, M., George, R., Foden, J., & Etheridge, M. (2007). U-series isotope and geodynamic constraints on mantle melting processes beneath the newer volcanic province in South Australia. *Earth and Planetary Science Letters*, *261*(3–4), 517–533. https://doi.org/10.1016/j.epsl.2007.07.006

Ellis, D. J. (1976). High pressure cognate inclusions in the newer volcanics of Victoria. *Contributions to Mineralogy and Petrology*, *58*(2), 149–180. https://doi.org/10.1007/BF00382183

Everard, J., Calver, C., Pemberton, J., Taheri, J., & Dixon, G. (1997). Geology of the islands of southwestern Bass Strait (Vol. 3). Tasmanian Geological Survey.

Everard, J. L. (1989). Petrology of the tertiary basalt - Geological atlas 1:50 000 series. Sheet 36 (8015S). St Valentines. In D. B. Seymour (Ed.), *Explanatory report geological survey Tasmania* (pp. 79–142). Geological Survey of Tasmania.

Ewart, A. (1982). Petrogenesis of the tertiary anorogenic volcanic series of Southern Queensland, Australia, in the light of trace element geochemistry and O, Sr, and Pb isotopes. *Journal of Petrology*, *23*(3), 344–382. https://doi.org/10.1093/petrology/23.3.344

Ewart, A., Baxter, K., & Ross, J. A. (1980). The petrology and petrogenesis of the Tertiary anorogenic mafic lavas of southern and central Queensland, Australia — Possible implications for crustal thickening. *Contributions to Mineralogy and Petrology*, *75*(2), 129–152. https://doi.org/10.1007/BF00389774

Ewart, A., Chappell, B., & Menzies, M. (1988). An overview of the geochemical and isotopic characteristics of the eastern Australian CainozoicVolcanic Provinces. *Journal of Petrology*, *1*, 225–273. https://doi.org/10.1093/petrology/special_volume.1.225

Ewart, A., Oversby, V. M., & Mateen, A. (1977). Petrology and isotope geochemisty of Tertiary lavas from the northern flank of the Tweed volcano, southeastern Queensland. *Journal of Petrology*, *18*(1), 73–113. https://doi.org/10.1093/petrology/18.1.73

Faiz, M., Saghafi, A., Sherwood, N., & Wang, I. (2007). The influence of petrological properties and burial history on coal seam methane reservoir characterization, Sydney Basin, Australia. *International Journal of Coal Geology*, *70*(1–3), 193–208. https://doi.org/10.1016/j.coal.2006.02.012

Fishwick, S., & Rawlinson, N. (2012). 3-D structure of the Australian lithosphere from evolving seismic datasets. *Australian Journal of Earth Sciences*, *59*(6), 809–826. https://doi.org/10.1080/08120099.2012.702319

Foden, J., Song, S. H., Turner, S., Elburg, M., Smith, P., Van der Steldt, B., & Van Penglis, D. (2002). Geochemical evolution of lithospheric mantle beneath SE South Australia. *Chemical Geology*, *182*(2–4), 663–695. https://doi.org/10.1016/s0009-2541(01)00347-3

Foley, S. (1992). Vein-plus-wall-rock melting mechanisms in the lithosphere and the origin of potassic alkaline magmas. *Lithos*, *28*(3–6), 435–453. https://doi.org/10.1016/0024-4937(92)90018-t

French, S. W., & Romanowicz, B. (2015). Broad plumes rooted at the base of the Earth's mantle beneath major hotspots. *Nature*, *525*(7567), 95–99. https://doi.org/10.1038/nature14876

Frey, F., Green, D., & Roy, S. (1978). Integrated models of basalt petrogenesis: A study of quartz tholeiites to olivine melilitites from south eastern Australia utilizing geochemical and experimental petrological data. *Journal of Petrology*, *19*(3), 463–513. https://doi.org/10.1093/petrology/19.3.463

Gaina, C., Müller, D. R., Royer, J.-Y., Stock, J., Hardebeck, J., & Symonds, P. (1998). The tectonic history of the Tasman Sea: A puzzle with 13 pieces. *Journal of Geophysical Research*, *103*(B6), 12413–12433. https://doi.org/10.1029/98jb00386

Gast, P. W. (1968). Trace element fractionation and the origin of tholeiitic and alkaline magma types. *Geochimica et Cosmochimica Acta*, *32*(10), 1057–1086.

Ghorbani, M. R., & Middlemost, E. A. (2000). Geochemistry of pyroxene inclusions from the Warrumbungle Volcano, New South Wales, Australia. *American Mineralogist*, *85*(10), 1349–1367. https://doi.org/10.2138/am-2000-1003

Gibson, D. L. (2007). Potassium-argon ages of late Mesozoic and Cainozoic igneous rocks of Eastern Australia (Vol.193). CSIRO Division of Exploration and Mining.

Gray, C., & McDougall, I. (2009). K-Ar geochronology of basalt petrogenesis, newer volcanic province, Victoria. *Australian Journal of Earth Sciences*, *56*(2), 245–258. https://doi.org/10.1080/08120090802547066

Griffin, T., & McDougall, I. (1975). Geochronology of the Cainozoic McBride volcanic province, northern Queensland. *Journal of the Geological Society of Australia*, *22*(4), 387–396. https://doi.org/10.1080/00167617508728905

Griffin, W., Wass, S., & Hollis, J. (1984). Ultramafic xenoliths from Bullenmerri and Gnotuk maars, Victoria, Australia: Petrology of a sub-continental crust-mantle transition. *Journal of Petrology*, *25*(1), 53–87. https://doi.org/10.1093/petrology/25.1.53

Griffin, W. L., Sutherland, F. L., & Hollis, J. D. (1987). Geothermal profile and crust-mantle transition beneath east-central Queensland: Volcanology, xenolith petrology and seismic data. *Journal of Volcanology and Geothermal Research*, *31*(3–4), 177–203. https://doi.org/10.1016/0377-0273(87)90067-9

Gurnis, M., Müller, R. D., & Moresi, L. (1998). Cretaceous vertical motion of Australia and the Australian-Antarctic discordance. *Science*, *279*(5356), 1499–1504. https://doi.org/10.1126/science.279.5356.1499

Hare, A., Cas, R., Musgrave, R., & Phillips, D. (2005). Magnetic and chemical stratigraphy for the Werribee Plains basaltic lava flow-field, Newer Volcanics Province, southeast Australia: Implications for eruption frequency. *Australian Journal of Earth Sciences*, *52*(1), 41–57. https://doi.org/10.1080/08120090500100069

Hill, S. (1999). Mesozoic regolith and palaeolandscape features in southeastern Australia: Significance for interpretations of denudation and highland evolution. *Australian Journal of Earth Sciences*, *46*(2), 217–232. https://doi.org/10.1046/j.1440-0952.1999.00705.x

Hoggard, M. J., Czarnota, K., Richards, F. D., Huston, D. L., Jaques, A. L., & Ghelichkhan, S. (2020). Global distribution of sediment-hosted metals controlled by craton edge stability. *Nature Geoscience*, *13*(7), 504–510. https://doi.org/10.1038/s41561-020-0593-2

Hoggard, M. J., White, N., & Al-Attar, D. (2016). Global dynamic topography observations reveal limited influence of large-scale mantle flow. *Nature Geoscience*, *9*, 456–463. https://doi.org/10.1038/ngeo2709

Hoggard, M. J., Winterbourne, J., Czarnota, K., & White, N. (2017). Oceanic residual depth measurements, the plate cooling model and global dynamic topography. *Journal of Geophysical Research: Solid Earth*, *122*(3), 2328–2372. https://doi.org/10.1002/2016JB013457

Holdgate, G., Wallace, M., Gallagher, S., Wagstaff, B., & Moore, D. (2008). No mountains to snow on: Major post-Eocene uplift of the East Victoria Highlands; evidence from Cenozoic deposits. *Australian Journal of Earth Sciences*, *55*(2), 211–234. https://doi.org/10.1080/08120090701689373

Irving, A., & Menzies, M. (1991). Isotopic evidence for variably enriched MORB lithospheric mantle in xenoliths from North Queensland, Australia. In International kimberlite conference: Extended abstracts (Vol. 5, pp. 186–187).

Jennings, E. S., & Holland, T. J. B. (2015). A simple thermodynamic model for melting of peridotite in the system NCFMASOCr. *Journal of Petrology*, *56*(5), 869–892. https://doi.org/10.1093/petrology/egv020

Johnson, R. W. (1989). *Intraplate volcanism in eastern Australian and New Zealand*. Press Syndicate of the University of Cambridge.

Jones, I., Ubide, T., Crossingham, T., Wilding, B., & Verdel, C. (2020). Evidence of a common source component for east Australian Cenozoic mafic magmatism. *Lithos*, *354*, 105254. https://doi.org/10.1016/j.lithos.2019.105254

Jones, I., Verdel, C., Crossingham, T., & Vasconcelos, P. (2017). Animated reconstructions of the Late Cretaceous to Cenozoic northward migration of Australia, and implications for the generation of east Australian mafic magmatism. *Geosphere*, *13*(2), 460–481. https://doi.org/10.1130/ges01405.1

Jones, I. M. (2018). *Evolution and migration of Cenozoic Australia: Precision $^{40}Ar/^{39}Ar$ geochronology, geochemistry and paleomagnetic data from east Australian Cenozoic magmas*. University of Queensland.

Jordan, S. C., Jowitt, S. M., & Cas, R. A. F. (2015). Origin of temporal-compositional variations during the eruption of Lake Purrumbete Maar, Newer Volcanics Province, southeastern Australia. *Bulletin of Volcanology*, *77*(1), 883. https://doi.org/10.1007/s00445-014-0883-x

Katz, R. F., Spiegelmann, M., & Langmuir, C. H. (2003). A new parameterization of hydrous mantle melting. *Geochemistry, Geophysics, Geosystems*, *4*(9), 1073. https://doi.org/10.1029/2002GC000433

Kay, R. W., & Gast, P. W. (1973). The rare earth content and origin of alkali-rich basalts. *The Journal of Geology*, *81*(6), 653–682. https://doi.org/10.1086/627919

Kay, S. M., & Kay, R. W. (1983). Thermal history of the deep crust inferred from granulite xenoliths, Queensland, Australia. *American Journal of Sciences*, *283*, 486–513.

Kennett, B., & Davies, D. (2020). Intra-plate volcanism in North Queensland and eastern new Guinea: A cryptic mantle plume? *Gondwana Research*, *79*, 209–216. https://doi.org/10.1016/j.gr.2019.10.003

Kennett, B., Salmon, M., Saygin, E., & Group, A. W. (2011). AusMoho: The variation of Moho depth in Australia. *Geophysical Journal International*, *187*(2), 946–958. https://doi.org/10.1111/j.1365-246x.2011.05194.x

Kennett, B. L., Fichtner, A., Fishwick, S., & Yoshizawa, K. (2013). Australian seismological reference model (AuSREM): Mantle component. *Geophysical Journal International*, *192*(2), 871–887. https://doi.org/10.1093/gji/ggs065

Kim, D.-H., & So, B.-D. (2020). Effects of rheology and mantle temperature structure on edge-driven convection: Implications for partial melting and dynamic topography. *Physics of the Earth and Planetary Interiors*, *303*, 106487. https://doi.org/10.1016/j.pepi.2020.106487

Klein, E. M., & Langmuir, C. H. (1987). Global correlations of ocean ridge basalt chemistry with axial depth and crustal thickness. *Journal of Geophysical Research*, *92*(B8), 8089–8115. https://doi.org/10.1029/jb092ib08p08089

Klöcking, M., Hoggard, M., Tribaldos, V. R., Richards, F., Guimarães, A., Maclennan, J., & White, N. (2020). A tale of two domes: Neogene to recent volcanism and dynamic uplift of northeast Brazil and southwest Africa. *Earth and Planetary Science Letters*, *547*, 116464. https://doi.org/10.1016/j.epsl.2020.116464

Klöcking, M., White, N. J., Maclennan, J., McKenzie, D., & Fitton, J. G. (2018). Quantitative relationships between basalt geochemistry, shear wave velocity, and asthenospheric temperature beneath western North America. *Geochemistry, Geophysics, Geosystems*, *19*, 3376–3404. https://doi.org/10.1029/2018gc007559

Knutson, J. *Whole-rock geochemical data from eastern Australia's cenozoic volcanic provinces*. Geoscience Australia

Kohn, B., Gleadow, A., Brown, R., Gallagher, K., O'sullivan, P., & Foster, D. (2002). Shaping the Australian crust over the last 300 million years: Insights from fission track thermotectonic imaging and denudation studies of key terranes. *Australian Journal of Earth Sciences*, *49*(4), 697–717. https://doi.org/10.1046/j.1440-0952.2002.00942.x

Lee, C. T. A., Luffi, P., Plank, T., Dalton, H., & Leeman, W. P. (2009). Constraints on the depths and temperatures of basaltic magma generation on Earth and other terrestrial planets using new thermobarometers for mafic magmas. *Earth and Planetary Science Letters*, *279*(1–2), 20–33. https://doi.org/10.1016/j.epsl.2008.12.020

Lister, G., & Etheridge, M. (1989). Detachment models for uplift and volcanism in the Eastern Highlands, and their application to the origin of passive margin mountains. *Intraplate volcanism in eastern Australia and New Zealand*, 297–313.

Matchan, E. L., & Phillips, D. (2014). High precision multi-collector 40Ar/39Ar dating of young basalts: Mount Rouse volcano (SE Australia) revisited. *Quarterly Geochronology*, *22*, 57–64. https://doi.org/10.1016/j.quageo.2014.02.005

Mather, B. R., Müller, R. D., Seton, M., Ruttor, S., Nebel, O., & Mortimer, N. (2020). Intraplate volcanism triggered by bursts in slab flux. *Science Advances*, *6*(51), eabd0953. https://doi.org/10.1126/sciadv.abd0953

Mather, K. A., Pearson, D. G., McKenzie, D., Kjarsgaard, B. A., & Priestley, K. (2011). Constraints on the depth and thermal history of cratonic lithosphere from peridotite xenoliths, xenocrysts and seismology. *Lithos*, *125*(1–2), 729–742. https://doi.org/10.1016/j.lithos.2011.04.003

Matthews, K. J., Maloney, K. T., Zahirovic, S., Williams, S. E., Seton, M., & Mueller, R. D. (2016). Global plate boundary evolution and kinematics since the late Paleozoic. *Global and Planetary Change*, *146*, 226–250. https://doi.org/10.1016/j.gloplacha.2016.10.002

Matthews, S., Wong, K., Shorttle, O., Edmonds, M., & Maclennan, J. (2021). Do olivine crystallization temperatures faithfully record mantle temperature variability? *Geochemistry, Geophysics, Geosystems*, *22*, e2020GC009157. https://doi.org/10.1029/2020GC009157

McBride, J. S., Lambert, D. D., Nicholls, I. A., & Price, R. C. (2001). Osmium isotopic evidence for crust-mantle interaction in the genesis of continental intraplate basalts from the Newer Volcanics Province, Southeastern Australia. *Journal of Petrology*, *42*(6), 1197–1218. https://doi.org/10.1093/petrology/42.6.1197

McClenaghan, M. P., Turner, N. J., Baillie, P. W., Brown, A. V., Williams, P. R., & Moore, W. R. (1982). Geology of the Ringarooma–Boobyalla area. *Geological Survey Bulletin*, *61*.

McDonough, W., McCulloch, M., & Sun, S. (1985). Isotopic and geochemical systematics in Tertiary-Recent basalts from southeastern Australia and implications for the evolution of the sub-continental lithosphere. *Geochimica et Cosmochimica Acta*, *49*(10), 2051–2067. https://doi.org/10.1016/0016-7037(85)90063-8

McGee, B. M. (2005). *Characteristics and origin of the Weldborough sapphire, NE Tasmania*. University of Tasmania, School of Earth Science.

McKenzie, D., & Bickle, M. J. (1988). The volume and composition of melt generated by extension of the lithosphere. *Journal of Petrology*, *29*(3), 625–679. https://doi.org/10.1093/petrology/29.3.625

McKenzie, D., Jackson, J., & Priestley, K. (2005). Thermal structure of oceanic and continental lithosphere. *Earth and Planetary Science Letters*, *233*(3–4), 337–349. https://doi.org/10.1016/j.epsl.2005.02.005

McKenzie, D., & O'Nions, R. K. (1991). Partial melt distributions from inversion of rare-earth element concentrations. *Journal of Petrology*, *32*(5), 1021–1091. https://doi.org/10.1093/petrology/32.5.1021

McKenzie, D., & O'Nions, R. K. (1995). The source regions of ocean island basalts. *Journal of Petrology*, *36*(1), 133–159. https://doi.org/10.1093/petrology/36.1.133

McQueen, K. G., Gonzalez, O. R., Roach, I. C., Pillans, B. J., Dunlap, W. J., & Smith, M. L. (2007). Landscape and regolith features related to Miocene leucitite flows, El Capitan northest of Cobar, New South Wales. *Australian Journal of Earth Sciences*, *54*(1), 1–17. https://doi.org/10.1080/08120090600923311

Menzies, M. A., & Wass, S. Y. (1983). CO_2-and LREE-rich mantle below eastern Australia: A REE and isotopic study of alkaline magmas and apatite-rich mantle xenoliths from the Southern Highlands Province, Australia. *Earth and Planetary Science Letters*, *65*(2), 287–302. https://doi.org/10.1016/0012-821x(83)90167-x

Michael, P. (1995). Regionally distinctive sources of depleted MORB: Evidence from trace elements and H₂O. *Earth and Planetary Science Letters*, *131*(3–4), 301–320. https://doi.org/10.1016/0012-821X(95)00023-6

Morgan, W. J. (1972). Deep mantle convection plumes and plate motions. *AAPG Bulletin*, *56*(2), 203–213. https://doi.org/10.1306/819a3e50-16c5-11d7-8645000102c1865d

Morris, P. A. (1986). Constraints on the origin of mafic alkaline volcanics and included xenoliths from Oberon, New South Wales, Australia. *Contributions to Mineralogy and Petrology*, *93*, 207–214. https://doi.org/10.1007/bf00371322

Müller, R. D., Flament, N., Matthews, K. J., Williams, S. E., & Gurnis, M. (2016). Formation of Australian continental margin highlands driven by plate–mantle interaction. *Earth and Planetary Science Letters*, *441*, 60–70. https://doi.org/10.1016/j.epsl.2016.02.025

Müller, R. D., Gaina, C., & Clark, S. (2000). Seafloor spreading around Australia. Billion-year earth history of Australia and neighbors in Gondwanaland, 18–28.

Müller, R. D., Lim, V. S., & Isern, A. R. (2000). Late Tertiary tectonic subsidence on the northeast Australian passive margin: Response to dynamic topography? *Marine Geology*, *162*(2–4), 337–352. https://doi.org/10.1016/s0025-3227(99)00089-4

Nasir, S. J., Everard, J. L., McClenaghan, M. P., Bombardieri, D., & Worthing, M. A. (2010). The petrology of high pressure xenoliths and associated Cenozoic basalts from Northeastern Tasmania. *Lithos*, *118*(1–2), 35–49. https://doi.org/10.1016/j.lithos.2010.03.012

Nelson, D. R., McCulloch, M. T., & Sun, S.-S. (1986). The origins of ultrapotassic rocks as inferred from Sr, Nd and Pb isotopes. *Geochimica et Cosmochimica Acta*, *50*(2), 231–245. https://doi.org/10.1016/0016-7037(86)90172-9

Nickel, K., & Green, D. (1985). Empirical geothermobarometry for garnet peridotites and implications for the nature of the lithosphere, kimberlites and diamonds. *Earth and Planetary Science Letters*, *73*(1), 158–170. https://doi.org/10.1016/0012-821x(85)90043-3

Nimis, P., & Taylor, W. R. (2000). Single clinopyroxene thermobarometry for garnet peridotites. Part I. Calibration and testing of a Cr-in-Cpx barometer and an enstatite-in-Cpx thermometer. *Contributions to Mineralogy and Petrology*, *139*(5), 541–554. https://doi.org/10.1007/s004100000156

O'Reilly, S. Y., & Griffin, W. (1984). Sr isotopic heterogeneity in primitive basaltic rocks, southeastern Australia: Correlation with mantle metasomatism. *Contributions to Mineralogy and Petrology*, *87*(3), 220–230. https://doi.org/10.1007/BF00373055

O'Reilly, S. Y., & Griffin, W. (1985). A xenolith-derived geotherm for southeastern Australia and its geophysical implications. *Tectonophysics*, *111*(1–2), 41–63. https://doi.org/10.1016/0040-1951(85)90065-4

O'Reilly, S. Y., & Griffin, W. (1988). Mantle metasomatism beneath western Victoria, Australia: I. Metasomatic processes in Cr-diopside lherzolites. *Geochimica et Cosmochimica Acta*, *52*(2), 433–447. https://doi.org/10.1016/0016-7037(88)90099-3

O'Reilly, S. Y., & Zhang, M. (1995). Geochemical characteristics of lava-field basalts from eastern Australia and inferred sources: Connections with the subcontinental lithospheric mantle? *Contributions to Mineral Petrology*, *121*, 148–170. https://doi.org/10.1007/s004100050096

O'Sullivan, P., Kohn, B., Foster, D., & Gleadow, A. (1995). Fission track data from the Bathurst Batholith: Evidence for rapid mid-Cretaceous uplift and erosion within the eastern highlands of Australia. *Australian Journal of Earth Sciences*, *42*(6), 597–607. https://doi.org/10.1080/08120099508728228

O'Sullivan, P., Mitchell, M., O'Sullivan, A., Kohn, B., & Gleadow, A. (2000). Thermotectonic history of the Bassian Rise, Australia: Implications for the breakup of eastern Gondwana along Australia's southeastern margins. *Earth and Planetary Science Letters*, *182*(1), 31–47. https://doi.org/10.1016/S0012-821X(00)00232-6

Paul, B., Hergt, J., & Woodhead, J. (2005). Mantle heterogeneity beneath the Cenozoic volcanic provinces of central Victoria inferred from trace-element and Sr, Nd, Pb, and Hf isotope data. *Australian Journal of Earth Sciences*, *52*(2), 243–260. https://doi.org/10.1080/08120090500139448

Price, R., Gray, C., & Frey, F. (1997). Strontium isotopic and trace element heterogeneity in the plains basalts of the Newer Volcanic Province, Victoria, Australia. *Geochimica et Cosmochimica Acta*, *61*(1), 171–192. https://doi.org/10.1016/s0016-7037(96)00318-3

Price, R. C., Gray, C. M., Wilson, R. E., Frey, F. A., & Taylor, S. R. (1991). The effects of weathering on rare-earth element, Y and Ba abundances in Tertiary basalts from southeastern Australia. *Chemical Geology*, *93*(3–4), 245–265. https://doi.org/10.1016/0009-2541(91)90117-A

Price, R. C., Nicholls, I. A., & Day, A. (2014). Lithospheric influences on magma compositions of late Mesozoic and Cenozoic intraplate basalts (the Older Volcanics) of Victoria, south-eastern Australia. *Lithos*, *206–207*(1), 179–200. https://doi.org/10.1016/j.lithos.2014.07.027

Priestley, K., & McKenzie, D. (2013). The relationship between shear wave velocity, temperature, attenuation and viscosity in the shallow part of the mantle. *Earth and Planetary Science Letters*, *381*, 78–91. https://doi.org/10.1016/j.epsl.2013.08.022

Rawlinson, N., Davies, D., & Pilia, S. (2017). The mechanisms underpinning Cenozoic intraplate volcanism in eastern Australia: Insights from seismic tomography and geodynamic modeling. *Geophysical Research Letters*, *44*(19), 9681–9690. https://doi.org/10.1002/2017gl074911

Raymond, O., Liu, S., Gallagher, R., Zhang, W., & Highet, L. (2012). *Surface geology of Australia 1:1 million scale dataset 2012 edition (Tech. Rep.)*. Commonwealth of Australia.

Richards, F. D., Hoggard, M. J., Cowton, L., & White, N. J. (2018). Reassessing the thermal structure of oceanic lithosphere with revised global inventories of basement depths and heat flow measurements. *Journal of Geophysical Research: Solid Earth*, *123*, 9136–9161. https://doi.org/10.1029/2018jb015998

Richards, F. D., Hoggard, M. J., White, N., & Ghelichkhan, S. (2020). Quantifying the relationship between short-wavelength dynamic topography and thermomechanical structure of the upper mantle using calibrated parameterization of anelasticity. *Journal of Geophysical Research: Solid Earth*, *125*, e2019JB019062. https://doi.org/10.1029/2019JB019062

Roach, I. C. (1999). *The setting, structural control, geochemistry and mantle source of the Monaro volcanic province, southeastern New South Wales, Australia*. University of Canberra.

Roach, I. C. (2004). Mineralogy, textures and P–T relationships of a suite of xenoliths from the Monaro volcanic province, New South Wales, Australia. *Journal of Petrology*, *45*(4), 739–758. https://doi.org/10.1093/petrology/egg108

Salles, T., Flament, N., & Müller, D. (2017). Influence of mantle flow on the drainage of eastern Australia since the Jurassic period. *Geochemistry, Geophysics, Geosystems*, *18*(1), 280–305. https://doi.org/10.1002/2016gc006617

Sandiford, M. (2007). The tilting continent: A new constraint on the dynamic topographic field from Australia. *Earth and Planetary Science Letters*, *261*(1–2), 152–163. https://doi.org/10.1016/j.epsl.2007.06.023

Sandiford, M., Wallace, M., & Coblentz, D. (2004). Origin of the in situ stress field in south-eastern Australia. *Basin Research*, *16*(3), 325–338. https://doi.org/10.1111/j.1365-2117.2004.00235.x

Schaeffer, A. J., & Lebedev, S. (2013). Global shear speed structure of the upper mantle and transition zone. *Geophysical Journal International*, *194*(1), 417–449. https://doi.org/10.1093/gji/ggt095

Shao, F., Niu, Y., Regelous, M., & Zhu, D.-C. (2015). Petrogenesis of peralkaline rhyolites in an intra-plate setting: Glass house mountains, southeast Queensland, Australia. *Lithos*, *216*, 196–210. https://doi.org/10.1016/j.lithos.2014.12.015

Shea, J. J., & Foley, S. F. (2019). Evidence for a carbonatite-influenced source assemblage for intraplate basalts from the Buckland volcanic province, Queensland, Australia. *Minerals*, *9*(9), 546. https://doi.org/10.3390/min9090546

Shorttle, O., Maclennan, J., & Lambart, S. (2014). Quantifying lithological variability in the mantle. *Earth and Planetary Science Letters*, *395*, 24–40. https://doi.org/10.1016/j.epsl.2014.03.040

Stephenson, P., Burch-Johnston, A., Stanton, D., & Whitehead, P. (1998). Three long lava flows in north Queensland. *Journal of Geophysical Research*, *103*(B11), 27359–27370. https://doi.org/10.1029/98jb01670

Stephenson, P., & Griffith, T. (1976). *Cainozoic volcanicity North Queensland*.

Stephenson, P., Zhang, M., & Spry, M. (2000). Fractionation modeling of segregations in the Toomba Basalt, north Queensland. *Australian Journal of Earth Sciences*, *47*(2), 291–300. https://doi.org/10.1046/j.1440-0952.2000.00780.x

Stephenson, R., & Lambeck, K. (1985). Erosion-isostatic rebound models for uplift: An application to south-eastern Australia. *Geophysical Journal International*, *82*(1), 31–55. https://doi.org/10.1111/j.1365-246x.1985.tb05127.x

Stolz, A. (1985). The role of fractional crystallization in the evolution of the Nandewar Volcano, north-eastern New South Wales, Australia. *Journal of Petrology*, *26*(4), 1002–1026. https://doi.org/10.1093/petrology/26.4.1002

Stolz, A. (1987). Fluid activity in the lower crust and upper mantle: Mineralogical evidence bearing on the origin of amphibole and scapolite in ultramafic and mafic granulite xenoliths. *Mineralogical Magazine*, *51*(363), 719–732. https://doi.org/10.1180/minmag.1987.051.363.13

Sutherland, F. L. (1989). Tertiary volcanism. In C. F. Burrett & E. L. Martin (Eds.), *Geology and mineral resources of Tasmania* (pp. 383–386). A bicentennial.

Sutherland, F. L. (1989). Tasmania and bass strait. In *Intraplate volcanism in eastern Australia and New Zealand* (pp. 143–149). Cambridge University.

Sutherland, F. L. (1998). Origin of north Queensland Cenozoic volcanism: Relationships to long lava flow basaltic fields, Australia. *Journal of Geophysical Research*, *103*(B11), 27347–27358. https://doi.org/10.1029/97jb03578

Sutherland, F. L. (2003). Eastern Australian rift margins and the Indian-Pacific mantle boundary. *Evolution and dynamics of the Australian Plate*, *372*, 203. https://doi.org/10.1130/0-8137-2372-8.203

Sutherland, F. L. (2004). *Cenozoic basalts, Tasmania: Landscapes, exposures, ages, petrography, geochemistry, entrainments and petrogenesis: Field guide A5: 17 AGC: Dynamic Earth: Past, present and future 2004: 17th Australian geological convention, Hobart: [programs and Abstracts]*. Geological Society of Australia.

Sutherland, F. L., Ewart, A., Raynor, L. R., Hollis, J. D., & McDonough, W. D. (1989). Tertiary basaltic magmas and the Tasmanian lithosphere. In Geology and Mineral Resources of Tasmania (Vol. 15, pp. 386–438). Geological Society of Australia Special Publication. https://doi.org/10.1007/978-1-349-07870-7_19

Sutherland, F. L., & Fanning, C. (2001). Gem-bearing basaltic volcanism, Barrington, New South Wales: Cenozoic evolution, based on basalt K–Ar ages and zircon fission track and U–Pb isotope dating. *Australian Journal of Earth Sciences*, *48*(2), 221–237. https://doi.org/10.1046/j.1440-0952.2001.00851.x

Sutherland, F. L., Graham, I., Forsyth, S., Zwingmann, H., & Everard, J. (2006). The Tamar trough revisited: Correlations between sedimentary beds, basalts, their ages and valley evolution, North Tasmania. *Papers and proceedings of the Royal Society of Tasmania*, *140*, 49, 74. https://doi.org/10.26749/rstpp.140.49

Sutherland, F. L., Graham, I. T., Hollis, J. D., Meffre, S., Zwingmann, H., Jourdan, F., & Pogson, R. E. (2014). Multiple felsic events within post-10 Ma volcanism, Southeast Australia: Inputs in appraising proposed magmatic models. *Australian Journal of Earth Sciences*, *61*(2), 241–267. https://doi.org/10.1080/08120099.2014.883640

Sutherland, F. L., Graham, I. T., Meffre, S., Zwingmann, H., & Pogson, R. E. (2012). Passive-margin prolonged volcanism, East Australian Plate: Outbursts, progressions, plate controls and suggested causes. *Australian Journal of Earth Sciences*, *59*(7), 983–1005. https://doi.org/10.1080/08120099.2012.688293

Sutherland, F. L., Graham, I. T., Pogson, R. E., Schwarz, D., Webb, G. B., Coenraads, R. R., et al. (2002). The Tumbarumba basaltic gem field, New South Wales: In relation to sapphire-ruby deposits of eastern Australia. *Records of the Australian Museum*, *54*(2), 215–248. https://doi.org/10.3853/j.0067-1975.54.2002.1358

Sutherland, F. L., Hendry, D. F., Barron, B. J., Matthews, W. L., & Hollis, J. D. (1996). An unusual Tasmanian Tertiary basalt sequence, near Boat Harbor, Northwest Tasmania. *Australian Museum*, *48*, 131–161. https://doi.org/10.3853/j.0067-1975.48.1996.285

Sutherland, F. L., Hollis, J. D., & Barron, L. M. (1984). Garnet lherzolite and other inclusions from a basalt flow, Bow Hill, Tasmania. In Developments in petrology (Vol. 11, pp. 145–160). Elsevier. https://doi.org/10.1016/b978-0-444-42274-3.50019-6

Taylor, G., Taylor, G., Bink, M., Foudoulis, C., Gordon, I., Hedstrom, J., et al. 1985). Pre-basaltic topography of the Northern Monaro and its implications. *Australian Journal of Earth Sciences*, *32*(1), 65–71. https://doi.org/10.1080/08120098508729313

Vandenberg, A. (2010). Paleogene basalts prove early uplift of Victoria's Eastern Uplands. *Australian Journal of Earth Sciences*, *57*(3), 291–315. https://doi.org/10.1080/08120091003619225

Van der Beek, P. A., Braun, J., & Lambeck, K. (1999). Post-Palaeozoic uplift history of southeastern Australia revisited: Results from a process-based model of landscape evolution. *Australian Journal of Earth Sciences*, *46*(2), 157–172. https://doi.org/10.1046/j.1440-0952.1999.00701.x

Van Otterloo, J., Raveggi, M., Cas, R. A., & Maas, R. (2014). Polymagmatic activity at the monogenetic Mt Gambier volcanic complex in the Newer Volcanics Province, SE Australia: New insights into the occurrence of intraplate volcanic activity in Australia. *Journal of Petrology*, *55*(7), 1317–1351. https://doi.org/10.1093/petrology/egu026

Vasconcelos, P. M., Knesel, K. M., Cohen, B., & Heim, J. (2008). Geochronology of the Australian Cenozoic: A history of tectonic and igneous activity, weathering, erosion, and sedimentation. *Australian Journal of Earth Sciences*, *55*(6–7), 865–914. https://doi.org/10.1080/08120090802120120

Vickery, N. M., Dawson, M. W., Sivell, W. J., Malloch, K. R., & Dunlap, W. J. (2007). Cainozoic igneous rocks in the Bingara to Inverell area northeastern New South Wales. *Quarterly Notes of the Geological Society of New South Wales*, *123*, 1–27.

Wass, S. Y. (1980). Geochemistry and origin of xenolith-bearing and related alkali basaltic rocks from the Southern Highlands, New South Wales, Australia. *American Journal of Science*, *280*(A), 639–666.

Webb, J. (2017). Denudation history of the southeastern Highlands of Australia. *Australian Journal of Earth Sciences*, *64*(7), 841–850. https://doi.org/10.1080/08120099.2017.1384759

Wellman, P. (1979). On the Cainozoic uplift of the southeastern Australian highland. *Journal of the Geological Society of Australia*, *26*(1–2), 1–9. https://doi.org/10.1080/00167617908729097

Wellman, P. (1987). Eastern highlands of Australia; their uplift and erosion. *BMR Journal of Australian Geology and Geophysics*, *10*, 277–286.

Wellman, P., & McDougall, I. (1974). Cainozoic igneous activity in eastern australia. *Tectonophysics*, *23*(1–2), 49–65. https://doi.org/10.1016/0040-1951(74)90110-3

Westrenen, W., Wood, B. J., & Blundy, J. D. (2001). A predictive thermodynamic model of garnet–melt trace element partitioning. *Contributions to Mineralogy and Petrology*, *142*(2), 219–234. https://doi.org/10.1007/s004100100285

White, R. S., McKenzie, D., & O'Nions, R. K. (1992). Oceanic crustal thickness from seismic measurements and rare Earth element inversions. *Journal of Geophysical Research*, *97*, 19683–19715. https://doi.org/10.1029/92jb01749

Whitehead, P. (1991). The geology and geochemistry of Mt. Napier and Mt. Rouse, western Victoria. In The Cainozoic in Australia: A re-appraisal of the evidence (Vol. 18, pp. 309–320). Geological Society of Australia, Special Publications.

Whitehead, P., & Stephenson, P. (1998). Lava rise ridges of the Toomba basalt flow, north Queensland, Australia. *Journal of Geophysical Research*, *103*(B11), 27371–27382. https://doi.org/10.1029/98jb00029

Whitehead, P. W., Stephenson, P. J., McDougall, I., Hopkins, M. S., Graham, A. W., Collerson, K. D., & Johnson, D. P. (2007). Temporal development of the Atherton Basalt province, north Queensland. *Australian Journal of Earth Sciences*, *54*(5), 691–709. https://doi.org/10.1080/08120090701305236

Wood, B. J., & Blundy, J. D. (1997). A predictive model for rare earth element partitioning between clinopyroxene and anhydrous silicate melt. *Contributions to Mineralogy and Petrology*, *129*(2–3), 166–181. https://doi.org/10.1007/s004100050330

Wyatt, D., & Webb, A. (1970). Potassium-argon ages of some northern queensland basalts and an interpretation of late cainozoic history. *Journal of the Geological Society of Australia*, *17*(1), 39–51. https://doi.org/10.1080/00167617008728722

Yamauchi, H., & Takei, Y. (2016). Polycrystal anelasticity at near-solidus temperatures. *Journal of Geophysical Research: Solid Earth*, *121*(11), 7790–7820. https://doi.org/10.1002/2016JB013316

Young, R., & McDougall, I. (1982). Basalts and silcretes on the coast near Ulladulla, southern New South Wales. *Journal of the Geological Society of Australia*, *29*(3–4), 425–430. https://doi.org/10.1080/00167618208729224

Young, R., & McDougall, I. (1993). Long-term landscape evolution: Early Miocene and modern rivers in southern New South Wales, Australia. *The Journal of Geology*, *101*(1), 35–49. https://doi.org/10.1086/648195

Young, R., & Wray, R. (2000). Contribution to the theory of scarpland development from observations in central Queensland, Australia. *The Journal of Geology*, *108*(6), 705–719. https://doi.org/10.1086/317949

Zhang, M., & O'Reilly, S. Y. (1997). Multiple sources for basaltic rocks from Dubbo, eastern Australia: Geochemical evidence for plume-lithospheric mantle interaction. *Chemical Geology*, *136*(1–2), 33–54. https://doi.org/10.1016/S0009-2541(96)00130-1

Zhang, M., Stephenson, P., O'Reilly, S. Y., McCulloch, M. T., & Norman, M. (2001). Petrogenesis and geodynamic implications of late Cenozoic basalts in North Queensland, Australia: Trace-element and Sr–Nd–Pb isotope evidence. *Journal of Petrology*, *42*(4), 685–719. https://doi.org/10.1093/petrology/42.4.685

Zhang, W., Min, K., Bryan, S. E., Foster, D. A., Fielding, C. R., Allen, C., & Kerrison, A. (2019). Multiple post-depositional thermal events in the Drummond Basin, Australia: Evidence from apatite and zircon (UTh)/He thermochronology. *Tectonophysics*, *767*, 128146. https://doi.org/10.1016/j.tecto.2019.06.016